Article

# A neurotransmitter produced by gut bacteria modulates host sensory behaviour

https://doi.org/10.1038/s41586-020-2395-5

Received: 3 August 2019

Accepted: 27 March 2020

Published online: 17 June 2020

Check for updates

Michael P. O'Donnell[1]✉, Bennett W. Fox[2], Pin-Hao Chao[1], Frank C. Schroeder[2] & Piali Sengupta[1]✉

Animals coexist in commensal, pathogenic or mutualistic relationships with complex communities of diverse organisms, including microorganisms[1]. Some bacteria produce bioactive neurotransmitters that have previously been proposed to modulate nervous system activity and behaviours of their hosts[2,3]. However, the mechanistic basis of this microbiota–brain signalling and its physiological relevance are largely unknown. Here we show that in *Caenorhabditis elegans*, the neuromodulator tyramine produced by commensal *Providencia* bacteria, which colonize the gut, bypasses the requirement for host tyramine biosynthesis and manipulates a host sensory decision. Bacterially produced tyramine is probably converted to octopamine by the host tyramine β-hydroxylase enzyme. Octopamine, in turn, targets the OCTR-1 octopamine receptor on ASH nociceptive neurons to modulate an aversive olfactory response. We identify the genes that are required for tyramine biosynthesis in *Providencia*, and show that these genes are necessary for the modulation of host behaviour. We further find that *C. elegans* colonized by *Providencia* preferentially select these bacteria in food choice assays, and that this selection bias requires bacterially produced tyramine and host octopamine signalling. Our results demonstrate that a neurotransmitter produced by gut bacteria mimics the functions of the cognate host molecule to override host control of a sensory decision, and thereby promotes fitness of both the host and the microorganism.

The pathways that mediate chemical communication between gut-colonizing bacteria and host nervous systems are largely undescribed[3]. The nematode *C. elegans* has recently emerged as a powerful experimental system in which to study host–microorganism chemical communication[4]. Diverse populations of pathogenic and nonpathogenic bacteria colonize the intestine of *C. elegans* and serve as the primary food source of this nematode in the wild[5]. Exposure to pathogenic bacteria alters the olfactory behaviour of *C. elegans*[6], but whether commensal gut bacteria also modulate host behaviour is unknown.

## Gut bacteria alter olfactory behaviour

To identify modes of microbial influence on host behaviour, we screened nonpathogenic bacterial strains that are typically associated with wild nematodes[7] for their ability to influence the olfactory responses of *C. elegans*. In long-range population chemotaxis assays[8], adult hermaphrodite worms cocultivated on these bacterial strains exhibited robust attraction to a panel of attractive volatile odorants similar to the behaviours of worms grown on the standard food source *Escherichia coli* strain OP50 (Extended Data Fig. 1a). However, cocultivation with the *Providencia alcalifaciens* strain JUb39[7,9] resulted in decreased avoidance of the volatile repellent 1-octanol but not of the repellents 2-nonanone and 8 M glycerol, as compared to worms grown on OP50 (Fig. 1a, Extended Data Fig. 1b). Henceforth, we refer to this decreased avoidance as octanol modulation. Worms grown on PYb007, a strain of *Providencia rettgeri* that is distantly related to JUb39 and was isolated from nematodes in compost (Extended Data Fig. 1c), exhibited similar octanol modulation (Fig. 1b). These observations indicate that, upon coculture, multiple species of *Providencia* modulate octanol aversion in *C. elegans*.

Under specific conditions, food deprivation reduces octanol avoidance[10]. JUb39 has previously been categorized as a 'beneficial' bacterium that supports robust *C. elegans* growth and does not induce stress responses[7], which suggests that worms fed JUb39 are unlikely to be deprived of nutrition. Consistently, growth on JUb39 did not alter expression of a *tph-1*p*::gfp* fusion gene, which is a reporter of feeding state[11,12] (Extended Data Fig. 1d). Moreover, growth of *C. elegans* on the poor bacterial food source *Bacillus megaterium*[13] did not alter octanol avoidance (Fig. 1a). We infer that octanol modulation by *Providencia* is unlikely to be solely due to changes in feeding state.

Although OP50 is typically crushed by the pharyngeal grinder in young adult *C. elegans*[14], a subset of bacterial strains can bypass the grinder and survive in the worm intestine[7,15,16]. Feeding *C. elegans* with JUb39 pretreated with the antibiotic gentamicin eliminated octanol modulation (Fig. 1c). In addition, the exposure of worms grown on OP50 to odours derived from JUb39 or the pre-incubation of worms grown on

[1]Department of Biology, Brandeis University, Waltham, MA, USA. [2]Boyce Thompson Institute and Department of Chemistry and Chemical Biology, Cornell University, Ithaca, NY, USA.
✉e-mail: mikeod@brandeis.edu; sengupta@brandeis.edu

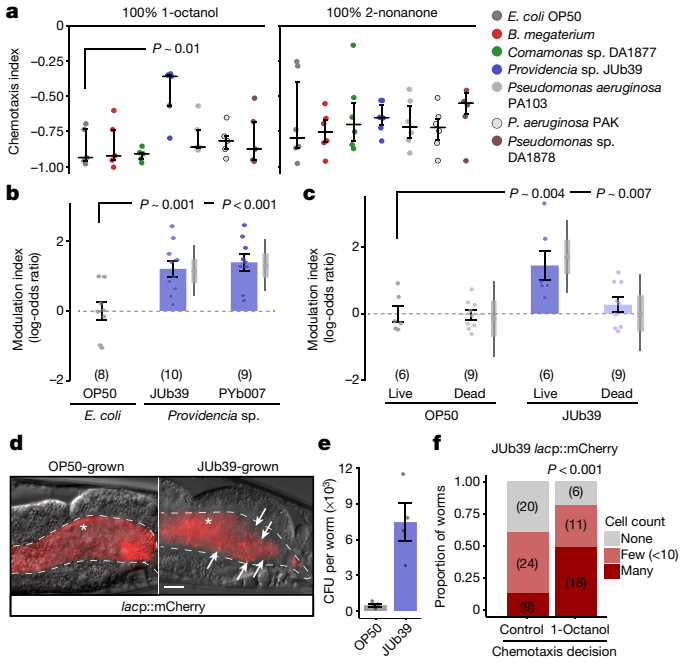


**Fig. 1 | *Providencia* colonizes the intestine of *C. elegans* and modulates octanol avoidance. a**, Long-range chemotaxis assays (Extended Data Fig. 1a) of *C. elegans* grown on the indicated bacterial strains to aversive odours. Chemotaxis index = (worms at odorant − worms at control)/total worms. Dots, chemotaxis index from single assays of approximately 100 worms each. Horizontal line, median; errors, 1st and 3rd quartiles. *P* value is derived from the *z*-statistic from a binomial general linearized mixed-effects model (GLMM) with random intercepts for assay plate and date, and with false discovery rate (FDR) for post hoc comparisons (two-sided test). $n = 5$ and 6 independent experiments for octanol and nonanone assays, respectively, over 3 days. **b**, **c**, Modulation index of worms in response to 100% octanol. 'Dead' (**c**) denotes bacteria that were pretreated with gentamicin. Modulation index, the log-odds ratio of the proportion of worms at octanol versus control of each condition normalized to worms grown on OP50 per independent day (grey dotted line). Positive numbers, reduced octanol avoidance. Errors are s.e.m. Grey thin and thick vertical bars, Bayesian 95% and 66% credible intervals, respectively. *P* values, two-sided GLMM with Dunnett-type (**b**) or Tukey-type (**c**) multivariate *t* adjustment. Numbers in parentheses, independent experiments over 3–5 days with approximately 100 worms each. **d**, mCherry-expressing bacteria in the posterior intestines of young adult worms. Arrows, intact cells; asterisks, diffuse intestinal fluorescence; dashed lines, intestinal boundary. Anterior is shown to the left. Scale bar, 10 µm. **e**, Intestinal bacterial load in worms grown on the indicated bacterial strains. Dots, estimation of bacterial load in colony-forming units (CFU) of 10 worms; $n = 4$ independent samples (Methods). Data are mean ± s.e.m. **f**, Proportion of worms that migrated to 100% octanol or control in chemotaxis assays with indicated distribution of mCherry-expressing JUb39 cells. Numbers in parentheses, number of worms; three independent assays. *P* value is derived from an ordinal regression *z*-statistic, using number of worms.

OP50 with JUb39-conditioned medium did not alter octanol responses (Extended Data Fig. 1e, f). These results suggest that *C. elegans* must ingest live JUb39 to induce octanol modulation.

To test whether colonization of the worm gut drives octanol modulation, we transformed OP50 and JUb39 with a plasmid that encodes a constitutively expressed mCherry fluorescent reporter. The guts of adult worms fed OP50 displayed only diffuse intestinal fluorescence (consistent with these bacteria being lysed), whereas the guts of worms fed JUb39 typically contained large numbers of intact rod-shaped cells that expressed mCherry (Fig. 1d). Large numbers of bacterial colonies could be isolated after crushing worms fed on JUb39—but not worms fed on OP50—after surface bleaching (Fig. 1e), which indicates that JUb39 is probably alive in the nematode intestine. JUb39 cells tended to be enriched in the posterior intestine (Fig. 1d), unlike the reported localization pattern of severely pathogenic bacteria[17]. Moreover, nematodes colonized by JUb39 did not exhibit phenotypes characteristic of pathogenic infection (such as anal swelling)[18] (Fig. 1d) and had a lifespan similar to that of worms fed OP50 (Extended Data Fig. 1g), further confirming that JUb39 is largely nonpathogenic to *C. elegans*. We performed additional chemotaxis assays with worms fed mCherry-labelled JUb39, and quantified intestinal bacterial cells in worms that had navigated towards either octanol or the control (ethanol). We found that worms navigating towards octanol consistently contained more gut bacteria (Fig. 1f). We conclude that JUb39 colonizes the worm gut, and that the extent of colonization is correlated with decision-making in response to octanol.

## *Providencia* bacteria produce tyramine

We next investigated the mechanistic basis for octanol modulation mediated by *Providencia*. Octanol avoidance is subject to extensive modulation directly and indirectly via multiple biogenic amines including tyramine and octopamine, as well as neuropeptides[10,19–23]. Tyramine is produced from tyrosine (L-Tyr) via the activity of a tyrosine decarboxylase (TDC) (encoded by *tdc-1* in *C. elegans*); tyramine is subsequently converted to octopamine via tyramine β-hydroxylase (encoded by *tbh-1*)[24] (Fig. 2a). Consequently, all *tbh-1*-mutant phenotypes that result from lack of octopamine are expected to be shared by *tdc-1*-mutant worms[24]. We found that although *tdc-1*-mutant worms grown on JUb39 exhibited octanol modulation, the modulation exhibited by *tbh-1*-mutant worms was reduced (Fig. 2b). Mutations in the tyrosine hydroxylase (encoded by *cat-2*[25]) and tryptophan hydroxylase (encoded by *tph-1*[26]) enzymes that are required for the production of dopamine and serotonin, respectively, in *C. elegans* did not affect octanol modulation (Fig. 2b). These results raise the possibility that octopamine—but not tyramine—produced by *C. elegans* is partly necessary for octanol modulation mediated by JUb39.

To account for these observations, we hypothesized that JUb39 may produce tyramine that functionally compensates for the host *tdc-1* mutation. *tdc-1*-mutant worms grown on OP50 have previously been reported to display more rapid aversive responses to dilute (30%) octanol, which is suppressed by exogenous tyramine[19]. Monoaminergic modulation of octanol responses has typically been assessed via the 'smell-on-a-stick' (SOS) short-range acute avoidance assay[10,27] performed on individual worms (Fig. 2c). In the SOS assay, the strength of avoidance is inversely correlated with reversal latency when the worm encounters the repellent as it is moving forward. To more easily enable comparisons with data from previously published work and to gain insight into the behavioural subprogrammes that are altered by JUb39, we performed all subsequent octanol behavioural experiments using SOS assays. As expected, *tdc-1*-mutant worms grown on OP50 responded more rapidly to 30% octanol than did wild-type worms in SOS assays (Fig. 2d). This enhanced aversion was suppressed upon growth on JUb39 (Fig. 2d). These results are consistent with the notion that bacterially produced tyramine functionally complements the loss of host-derived tyramine in driving a sensory behavioural decision.

We performed metabolomic analyses to test whether growth on JUb39 compensates for the loss of tyramine and its metabolites in *tdc-1*-mutant worms. Using high-performance liquid chromatography (HPLC) with high-resolution mass spectrometry[28] we found that *tdc-1*-mutant worms grown on OP50 were deficient in *N*-succinyl tyramine (as previously reported[24]) as well as in additional metabolites that appeared, on the basis of MS2 analysis, to be derived from tyramine (Fig. 2e, Extended Data Figs. 2–5). Metabolism of serotonin was largely unperturbed (Extended Data Fig. 6). Production of

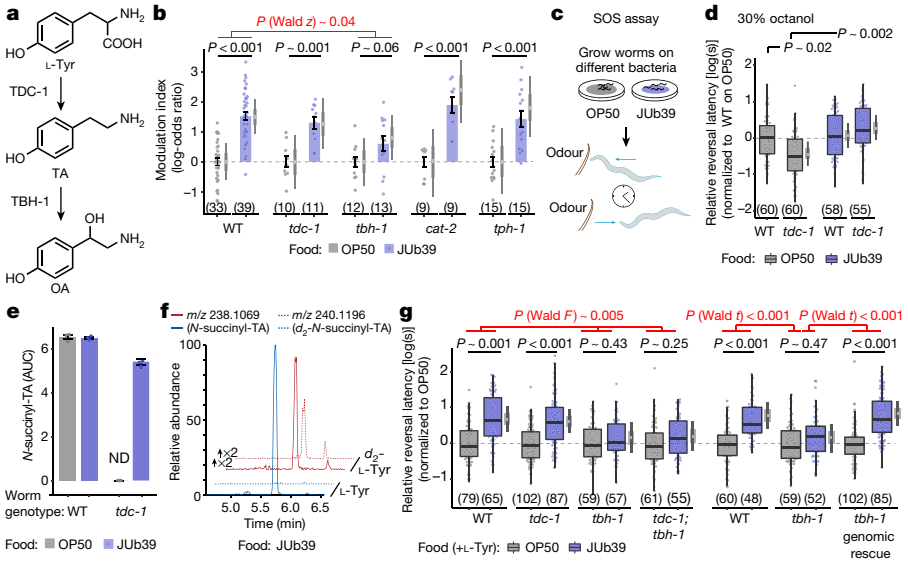


**Fig. 2 | Tyramine produced by *Providencia* compensates for the loss of *tdc-1* in *C. elegans*.** **a**, Biosynthesis of tyramine (TA) and octopamine (OA) in *C. elegans*[24]. **b**, Modulation index of worms in response to 100% octanol. Dots, individual chemotaxis assays with approximately 100 worms each. Numbers in parentheses, number of independent assays over at least three independent days. The *y* axis is on a log-odds (logit) scale, normalized to OP50 for each day (grey dashed lines). Errors are s.e.m. Grey thin and thick vertical bars, Bayesian 95% and 66% credible intervals, respectively. *P* values, GLMM with Dunnett-type multivariate *t* adjustment. *P* value in red, Wald *z*-statistic for the magnitude of the JUb39 effect in *tbh-1*-mutant worms compared to wild type (WT). **c**, Cartoon of SOS assay[10,27]. **d**, **g**, Reversal response latency of worms on nematode growth medium (NGM) without (**d**) or with (**g**) 0.5% L-Tyr in response to 30% (**d**) or 100% (**g**) octanol in SOS assays. Dots, response time of single worms. The *y* axis is $\log_{10}$-scaled, normalized to the indicated control group for each experimental day. Numbers in parentheses, number of worms tested in assays over at least three independent days. Box plot, median and quartiles; whiskers, data range (excluding outliers). Grey thin and thick vertical bars, Bayesian 95% and 66% credible intervals for the difference of means, respectively. *P* values, linear-mixed effects model (LMM) regression on log-transformed data. *P* values in red (**g**), Wald *F*-statistic (left) or Wald *t*-statistic (right) for the effect of the indicated genotypes on the magnitude of the JUb39 effect. Data from wild type in **g** (right) are repeated in Extended Data Fig. 7b. Alleles: *tbh-1(ok1196)* (**g**, left) and *tbh-1(n3247)* (**g**, right). **e**, Quantification of *N*-succinyl tyramine. Dots, area under the curve (AUC) from three biologically independent experiments. Data are mean ± s.e.m. ND, not detected. **f**, HPLC with mass spectrometry (HPLC–MS) (positive electrospray ionization mode (ESI+)) ion chromatograms for *N*-succinyl tyramine or $d_2$-*N*-succinyl tyramine in worms grown on JUb39 with the indicated amino acid supplementation. Chromatograms for worms fed $d_2$-L-Tyr are scaled twofold relative to worms fed L-Tyr. Statistical comparisons are two-sided.

these tyramine-derived metabolites was restored when *tdc-1*-mutant worms were grown on JUb39 (Fig. 2e, Extended Data Figs. 3, 4d, 5d). Metabolomic analysis of *tdc-1*-mutant worms grown on JUb39 supplemented with stable-isotope-labelled $d_2$-L-tyrosine confirmed de novo biosynthesis of the tyramine moiety (Fig. 2f). We did not detect either free tyramine or tyramine conjugates in the absence of *C. elegans*. We conclude that JUb39 in association with *C. elegans* produces tyramine that can compensate for the lack of endogenous tyramine production in *tdc-1*-mutant worms.

Although tyramine biosynthesis in bacteria has previously been demonstrated in some Gram-positive genera, production appears to be uncommon in Gram-negative bacteria (which include *Providencia*)[29,30]. Tyramine production in Gram-positive strains is induced upon supplementation with L-Tyr[31]. We found that growth on medium supplemented with L-Tyr enhanced octanol modulation by JUb39 in SOS assays (Extended Data Fig. 7a). Mutations in *tbh-1* fully suppressed octanol modulation in SOS assays, whereas *tdc-1*-mutant worms continued to exhibit robust octanol modulation (Fig. 2g), consistent with our observations in long-range chemotaxis assays (Fig. 2b). Moreover, the octanol avoidance behaviours of *tdc-1; tbh-1* double-mutant worms were similar to those of worms with mutations only in *tbh-1* (Fig. 2g). These results indicate that the lack of host-derived octopamine—and not the accumulation of tyramine owing to loss of TBH-1[24,28]—accounts for the reduced octanol modulation in *tbh-1*-mutant worms. Expression of wild-type genomic *tbh-1* sequences rescued octanol modulation in *tbh-1*-mutant worms (Fig. 2g). Consistent with a role for neuronal octopamine release in octanol modulation, worms with mutations in *cat-1*, which encodes a neuron-specific vesicular monoamine transporter[32], were also deficient in octanol modulation (Extended Data Fig. 7b).

## Bacterial decarboxylases generate tyramine

In both eukaryotes and bacteria, biogenic amines are typically generated from aromatic amino acids and L-glutamate by group-II aromatic-acid decarboxylase enzymes (AADCs)[33]. In Gram-positive *Enterococcus* and *Lactobacillus* bacteria, tyramine production is mediated by the *tyrDC* and *tyrP* genes (which encode the AADC TyrDC and the tyrosine permease, respectively) present in an operon; this operon is inducible by L-Tyr[34,35] (Fig. 3a, Extended Data Fig. 8a–c, Supplementary Table 1). Although genes related to the *Enterococcus tyrDC* and *tyrP* are largely absent in Gammaproteobacteria (Extended Data Fig. 8c), we confirmed the presence of homologous operons containing *tyrDC* and *tyrP* in JUb39 and PYb007 in de novo genome assemblies via whole-genome sequencing (Fig. 3a, Supplementary Table 1). We also identified *tyrDC* homologues in the genomes of additional members of the Morganellaceae family, although the operon structure was conserved in only a subset of these genomes (Fig. 3a, b, Supplementary Table 1).

The *Providencia* TyrDC is highly homologous to the enzyme in *Lactobacillus*, which has been well-characterized with respect to substrate specificity[36]. We performed protein modelling using the crystal structure of *Lactobacillus* TyrDC[36] as a guide (Methods), which indicated that JUb39 TyrDC shares most known catalytic sites with *Lactobacillus* TyrDC (Extended Data Fig. 8d). JUb39 TyrDC contains a substitution at A600 (S586 in *Lactobacillus* TyrDC) (Extended Data

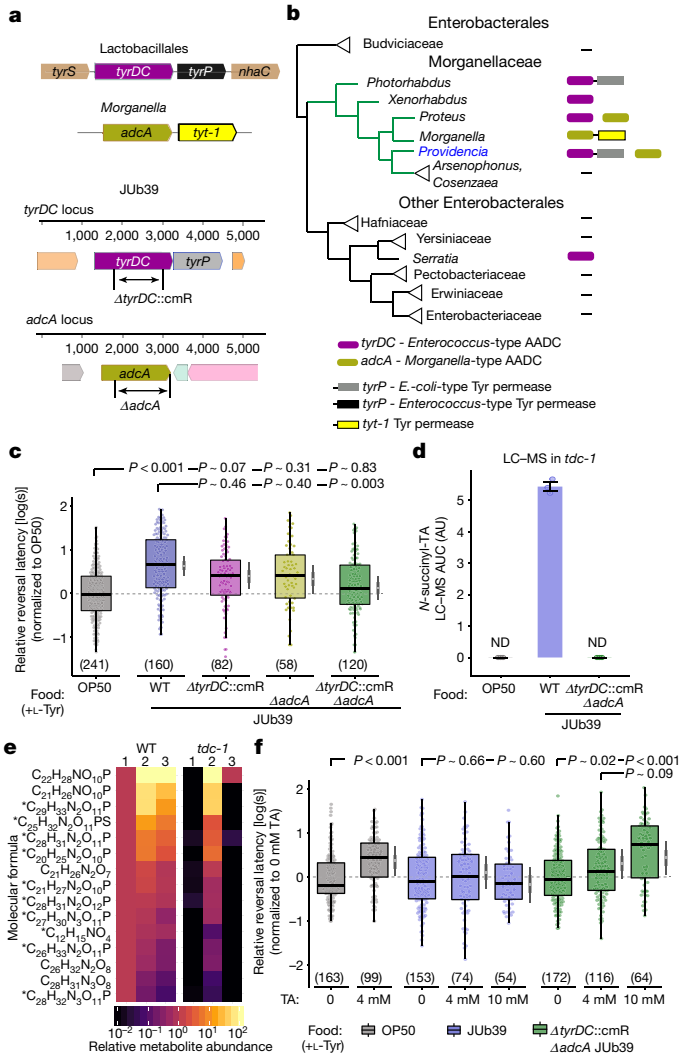


**Fig. 3 | Two AADCs in *Providencia* act redundantly to modulate octanol avoidance. a**, Cartoons depicting the *tyrDC* locus in Lactobacillales, the *adcA* locus in *Morganella* (top), and corresponding loci including engineered muations in JUb39 (bottom). **b**, Presence of *tyrDC*, *adcA*, *E.-coli*-type *tyrP* and *Morganella*-type *tyt-1* at the family and genus level among Enterobacterales. Linked boxes indicate organization in an operon. **c**, **f**, Reversal response latency of wild-type *C. elegans* grown on the indicated bacterial genotypes in NGM + 0.5% L-Tyr (**c**) or supplemented with the indicated concentrations of tyramine (**f**) to 100% octanol using SOS assays. Dots, response time of single worms. The *y* axis is $\log_{10}$-scaled and normalized to the indicated control group for each experimental day (grey dashed line). Numbers in parentheses, number of worms tested in assays over at least three independent days. Box plot, median and quartiles; whiskers, data range (excluding outliers). Grey thin and thick vertical bars at right, Bayesian 95% and 66% credible intervals for the difference of means, respectively. *P* values between indicated conditions are from an LMM with Tukey-type multivariate *t* adjustment. **d**, Quantification of *N*-succinyl tyramine in *tdc-1*-mutant worms grown on the indicated bacterial strains. OP50 and JUb39 data are repeated from Fig. 2e. Dots, AUC from each of three biologically independent experiments. Data are mean ± s.e.m. AU, arbitrary units; ND, not detected. **e**, Heat map showing mean abundance, relative to N2 worms grown on OP50, of tyramine-derived compounds of the indicated molecular formula detected in N2 wild-type and *tdc-1*-mutant worms grown on the indicated bacterial strains: 1, OP50; 2, JUb39; 3, *ΔtyrDC*::cmR *ΔadcA* JUb39. Means are calculated from three independent experiments. Asterisks indicate $d_2$-containing compounds confirmed using $d_2$-L-Tyr supplementation (Fig. 2f).

Fig. 8d), a variant that has previously been demonstrated to enhance the specific catalytic activity of *Lactobacillus* TyrDC for tyrosine[36]. We infer that JUb39 TyrDC probably generates tyramine from tyrosine.

Strains in the *Morganella* genus (Morganellaceae family) have previously been reported to produce tyramine under some conditions[29], despite having no discernible *tyrDC* orthologues (Fig. 3b, Extended Data Fig. 8a–c, Supplementary Table 1). Instead, we identified a gene in *Morganella* that encodes an AADC (which we name *adcA*) with approximately 29% and 27% sequence identity to *Enterococcus* TyrDC and human GAD67, respectively, in an operon upstream of a gene that encodes a putative tyrosine permease of the Tyt1 family[37] (Fig. 3a, b). An *adcA* homologue is also present in *Providencia* genomes (including in JUb39), but is not adjacent to a tyrosine transporter (Fig. 3a, b, Extended Data Fig. 8a–c, Supplementary Table 1). We conclude that *Providencia* encodes at least two AADCs with the potential to generate tyramine, and the phylogenetic incongruence suggests that both *tyrDC* and *adcA* genes in the Morganellaceae family may have either been lost or acquired via horizontal gene transfer.

To test whether one or both JUb39 AADCs are necessary for octanol modulation, we engineered deletions in JUb39 *tyrDC* and *adcA* (*ΔtyrDC*::cmR and *ΔadcA*, respectively) (Fig. 3a). Cultivation on each of the bacterial single mutants weakly decreased octanol modulation, whereas growth of wild-type *C. elegans* on the JUb39 *ΔtyrDC*::cmR *ΔadcA* double-knockout bacteria abolished octanol modulation (Fig. 3c). We confirmed that *ΔtyrDC*::cmR *ΔadcA* JUb39 colonizes the *C. elegans* gut (Extended Data Fig. 9a). In contrast to wild-type JUb39, comparative metabolomics analyses showed that *tdc-1*-mutant worms grown on the *ΔtyrDC*::cmR *ΔadcA* double-mutant JUb39 did not produce *N*-succinyl tyramine or other tyramine-derived metabolites (Fig. 3d, e, Extended Data Figs. 3, 4d, 5d). Octanol modulation was restored in wild-type *C. elegans* grown on *ΔtyrDC*::cmR *ΔadcA* JUb39 upon supplementation with tyramine (Fig. 3f). Moreover, although exogenous tyramine did not further increase octanol avoidance in wild-type worms grown on JUb39, tyramine supplementation was sufficient to induce octanol modulation in worms grown on OP50 (Fig. 3f). Together, these results indicate that tyramine produced by multiple AADCs in *Providencia* is both necessary and sufficient to modulate octanol avoidance by wild-type *C. elegans*.

Tyramine regulates behaviours such as egg-laying in *C. elegans*[24,38]. We asked whether tyramine produced by AADCs in *Providencia* is sufficient to suppress egg-laying defects of *tdc-1*-mutant worms, in addition to modulating octanol avoidance indirectly via octopamine. Consistent with previous reports[24], we found that *tdc-1*-mutant worms grown on OP50 contained on average younger eggs in utero than those of wild-type worms; however, growth on wild-type JUb39—but not on *ΔtyrDC*::cmR *ΔadcA* JUb39—suppressed this egg-laying defect of *tdc-1*-mutant worms (Extended Data Fig. 10). These results indicate that tyramine produced by JUb39 in worms complements multiple *tdc-1*-dependent phenotypes.

## Bacterial tyramine targets sensory neurons

We next sought to identify the molecular targets of *Providencia*-mediated octanol modulation in the host. The bilateral ASH nociceptive neurons in the head amphid organs of *C. elegans* have previously been implicated in sensing octanol[10,20,27]. These neurons express multiple tyramine and octopamine receptors, a subset of which is required for octanol modulation by these monoamines[19,39]. Among the genes encoding octopamine receptors expressed in ASH neurons, mutations in *octr-1*—but not *ser-3*—abolished the octanol modulation mediated by JUb39, without altering the extent of gut colonization (Fig. 4a, Extended Data Fig. 9). We also observed an effect on octanol modulation in worms with a mutation in *tyra-2* (which encodes a tyramine receptor), primarily due to decreased octanol avoidance upon growth on OP50 (4.3 ± 0.25 s for *tyra-2*-mutant worms versus 2.9 ± 0.13 s for

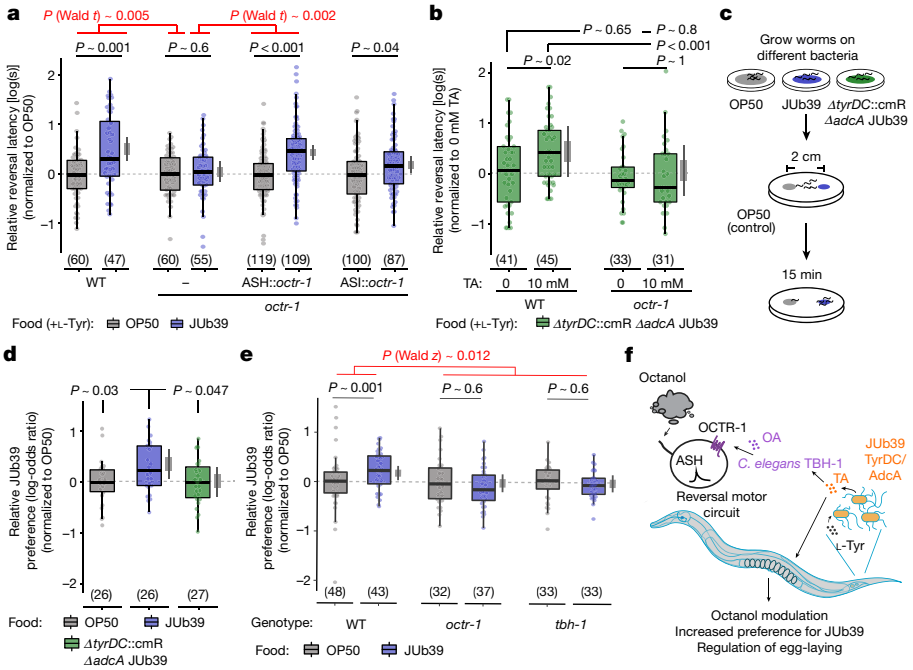


**Fig. 4 | Modulation of octanol avoidance by *Providencia* requires the OCTR-1 octopamine receptor in the ASH sensory neurons. a**, **b**, Reversal response latency of worms of the indicated genotypes grown on the indicated bacteria on NGM + 0.5% L-Tyr (**a**) and supplemented with the indicated concentrations of tyramine (**b**) to 100% octanol using SOS assays. Dots, response time of single worms. The *y* axis is $\log_{10}$-scaled and normalized to the indicated control group (**a**) or to the wild-type control (**b**) for each experimental day. Numbers in parentheses, number of worms tested in assays over at least three independent days. Wild-type *octr-1* sequences were expressed in ASH and ASI neurons under the *srv-11* and *srg-47* promoters, respectively. Box plot, median and quartiles; whiskers, data range (excluding outliers). Grey thin and thick vertical bars, Bayesian 95% and 66% credible intervals for the difference of means, respectively. *P* values between indicated conditions are from an LMM with Tukey-type multivariate *t* adjustment. *P* values in red, Wald *t*-statistic representing the genotype × food interaction effect relative to wild type. **c**, Cartoon depicting short-range bacterial choice assay. **d**, **e**, Relative preference index of wild-type or mutant worms grown on the indicated bacteria for the test bacteria JUb39. Data are normalized to the OP50 control condition for each genotype. Dots, single assays of at least 10 worms. Numbers in parentheses, number of assays over at least five independent days. The *y* axis is on a log-odds ratio (logit) scale. Errors are s.e.m. Grey thin and thick vertical bars, Bayesian 95% and 66% credible intervals, respectively. *P* values represent difference of means relative to worms grown on JUb39 from a GLMM with Dunnett-type multivariate *t* adjustment. *P* value in red, Wald *z*-statistic representing the genotype × food interaction effect relative to wild type (**e**). Allele used: *tbh-1(n3247)* (**e**). **f**, Cartoon of working model. OA, octopamine; TA, tyramine.

wild type) (Extended Data Fig. 9b). Expression of *octr-1* complementary DNA in ASH, but not ASI, sensory neurons fully restored octanol modulation (Fig. 4a). *octr-1*-mutant worms also lacked octanol modulation when grown on *ΔtyrDC*::cmR *ΔadcA* JUb39 supplemented with tyramine (Fig. 4b). OCTR-1 has previously been shown to inhibit innate immune responses to pathogens in *C. elegans*, via suppression of an unfolded-protein-response pathway[40]. However, previous observations that JUb39 does not induce the expression of genes associated with virulence, stress or unfolded protein response[7], our finding that it only minimally affects *C. elegans* longevity (Extended Data Fig. 1g) and the well-established role of ASH neurons in octopamine-modulated octanol avoidance[10,19–21] together suggest that the observed behavioural responses to octanol are unlikely to arise from changes in innate immune responses in worms grown on JUb39.

## Bacterial tyramine biases feeding choices

We next investigated the biological relevance of the JUb39-directed decrease in aversive olfactory responses by *C. elegans*. Although many Gram-negative enteric bacteria produce long-chain alcohols (including octanol)[41], whether *Providencia* produces this chemical is unknown. However, JUb39 and other *Providencia* strains produce the branched alcohol isoamyl alcohol, which is aversive to *C. elegans* when concentrated[42,43]. Similar to octanol, avoidance of high concentrations of isoamyl alcohol is also mediated by ASH sensory neurons[43]. We hypothesized that reduced avoidance of aversive alcohols or other odorants produced by JUb39 may preferentially bias *C. elegans* grown on JUb39 to select these bacteria in food choice assays (Fig. 4c). Indeed, worms grown on JUb39 preferred JUb39, whereas worms grown on OP50 showed only a slight preference for JUb39 in a short-range food choice assay (Fig. 4d). The bias towards JUb39 was largely eliminated in worms grown on *ΔtyrDC*::cmR *ΔadcA* JUb39 (Fig. 4d), as well as in *octr-1*- and *tbh-1*-mutant worms (Fig. 4e), which suggests that both bacterial tyramine production and host octopamine signalling are necessary for this food preference. Together, these results imply that tyramine produced by JUb39 in the worm intestine acts via host octopamine and the OCTR-1 octopamine receptor to reduce ASH-neuron-mediated avoidance of aversive cues produced by JUb39 (such as concentrated alcohols) and allow preferential selection of these bacteria (Fig. 4f).

## Discussion

Our observations support a model in which the neurotransmitter tyramine produced by intestinal *Providencia* bacteria can subvert host-dependent tyramine production to modulate multiple monoaminergic pathways and alter behaviour and physiology in *C. elegans*. Bacterially produced tyramine is converted to octopamine by *C. elegans* TBH-1; octopamine subsequently acts on the ASH neurons via the OCTR-1 octopamine receptor to decrease aversion of bacterially produced volatiles such as octanol, and alter food choices (Fig. 4f). We speculate that the preference for *Providencia* upon colonization of *C. elegans* by these bacteria promotes increased consumption that

leads to a stable association[5,44] and bacterial dispersal. As *Providencia* is a rich food source for *C. elegans*[7], this association may be mutually beneficial. Other metabolites from commensal bacteria have previously been shown to have a beneficial effect on feeding decisions as well as maintenance and dispersal of these bacteria in *Drosophila*[45–47], and intestinal bacteria can modulate satiety responses in mammals via mechanisms that are largely uncharacterized[48,49]. Our results describe a pathway by which neurotransmitters produced by natural commensal bacteria direct host sensory behavioural decisions by supplementing or compensating for the activity of key host biosynthetic enzymes, thereby altering the fitness of both host and microorganism.

## Online content

Any methods, additional references, Nature Research reporting summaries, source data, extended data, supplementary information, acknowledgements, peer review information; details of author contributions and competing interests; and statements of data and code availability are available at https://doi.org/10.1038/s41586-020-2395-5.


1. Douglas, A. E. *Fundamentals of Microbiome Science: How Microbes Shape Animal Biology* (Princeton Univ. Press, 2018).
2. Guo, R., Chen, L.-H., Xing, C. & Liu, T. Pain regulation by gut microbiota: molecular mechanisms and therapeutic potential. *Br. J. Anaesth*. **123**, 637–654 (2019).
3. Strandwitz, P. Neurotransmitter modulation by the gut microbiota. *Brain Res*. **1693** (Pt B), 128–133 (2018).
4. Zhang, J., Holdorf, A. D. & Walhout, A. J. *C. elegans* and its bacterial diet as a model for systems-level understanding of host–microbiota interactions. *Curr. Opin. Biotechnol*. **46**, 74–80 (2017).
5. Schulenburg, H. & Félix, M.-A. The natural biotic environment of *Caenorhabditis elegans*. *Genetics* **206**, 55–86 (2017).
6. Meisel, J. D. & Kim, D. H. Behavioral avoidance of pathogenic bacteria by *Caenorhabditis elegans*. *Trends Immunol*. **35**, 465–470 (2014).
7. Samuel, B. S., Rowedder, H., Braendle, C., Félix, M.-A. & Ruvkun, G. *Caenorhabditis elegans* responses to bacteria from its natural habitats. *Proc. Natl Acad. Sci. USA* **113**, E3941–E3949 (2016).
8. Bargmann, C. I., Hartwieg, E. & Horvitz, H. R. Odorant-selective genes and neurons mediate olfaction in *C. elegans*. *Cell* **74**, 515–527 (1993).
9. Song, B.-M., Faumont, S., Lockery, S. & Avery, L. Recognition of familiar food activates feeding via an endocrine serotonin signal in *Caenorhabditis elegans*. *eLife* **2**, e00329 (2013).
10. Chao, M. Y., Komatsu, H., Fukuto, H. S., Dionne, H. M. & Hart, A. C. Feeding status and serotonin rapidly and reversibly modulate a *Caenorhabditis elegans* chemosensory circuit. *Proc. Natl Acad. Sci. USA* **101**, 15512–15517 (2004).
11. Liang, B., Moussaif, M., Kuan, C.-J., Gargus, J. J. & Sze, J. Y. Serotonin targets the DAF-16/FOXO signaling pathway to modulate stress responses. *Cell Metab*. **4**, 429–440 (2006).
12. Entchev, E. V. et al. A gene-expression-based neural code for food abundance that modulates lifespan. *eLife* **4**, e06259 (2015).
13. Avery, L. & Shtonda, B. B. Food transport in the *C. elegans* pharynx. *J. Exp. Biol*. **206**, 2441–2457 (2003).
14. Avery, L. The genetics of feeding in *Caenorhabditis elegans*. *Genetics* **133**, 897–917 (1993).
15. Berg, M. et al. Assembly of the *Caenorhabditis elegans* gut microbiota from diverse soil microbial environments. *ISME J*. **10**, 1998–2009 (2016).
16. Dirksen, P. et al. The native microbiome of the nematode *Caenorhabditis elegans*: gateway to a new host–microbiome model. *BMC Biol*. **14**, 38 (2016).
17. Tan, M.-W., Mahajan-Miklos, S. & Ausubel, F. M. Killing of *Caenorhabditis elegans* by *Pseudomonas aeruginosa* used to model mammalian bacterial pathogenesis. *Proc. Natl Acad. Sci. USA* **96**, 715–720 (1999).
18. Irazoqui, J. E. et al. Distinct pathogenesis and host responses during infection of *C. elegans* by *P. aeruginosa* and *S. aureus*. *PLoS Pathog*. **6**, e1000982 (2010).
19. Wragg, R. T. et al. Tyramine and octopamine independently inhibit serotonin-stimulated aversive behaviors in *Caenorhabditis elegans* through two novel amine receptors. *J. Neurosci*. **27**, 13402–13412 (2007).
20. Mills, H. et al. Monoamines and neuropeptides interact to inhibit aversive behaviour in *Caenorhabditis elegans*. *EMBO J*. **31**, 667–678 (2012).
21. Harris, G. et al. The monoaminergic modulation of sensory-mediated aversive responses in *Caenorhabditis elegans* requires glutamatergic/peptidergic cotransmission. *J. Neurosci*. **30**, 7889–7899 (2010).
22. Ezak, M. J. & Ferkey, D. M. The *C. elegans* D2-like dopamine receptor DOP-3 decreases behavioral sensitivity to the olfactory stimulus 1-octanol. *PLoS ONE* **5**, e9487 (2010).
23. Ezcurra, M., Tanizawa, Y., Swoboda, P. & Schafer, W. R. Food sensitizes *C. elegans* avoidance behaviours through acute dopamine signalling. *EMBO J*. **30**, 1110–1122 (2011).
24. Alkema, M. J., Hunter-Ensor, M., Ringstad, N. & Horvitz, H. R. Tyramine functions independently of octopamine in the *Caenorhabditis elegans* nervous system. *Neuron* **46**, 247–260 (2005).
25. Lints, R. & Emmons, S. W. Patterning of dopaminergic neurotransmitter identity among *Caenorhabditis elegans* ray sensory neurons by a TGFβ family signaling pathway and a *Hox* gene. *Development* **126**, 5819–5831 (1999).
26. Sze, J. Y., Victor, M., Loer, C., Shi, Y. & Ruvkun, G. Food and metabolic signalling defects in a *Caenorhabditis elegans* serotonin-synthesis mutant. *Nature* **403**, 560–564 (2000).
27. Troemel, E. R., Chou, J. H., Dwyer, N. D., Colbert, H. A. & Bargmann, C. I. Divergent seven transmembrane receptors are candidate chemosensory receptors in *C. elegans*. *Cell* **83**, 207–218 (1995).
28. Artyukhin, A. B. et al. Succinylated octopamine ascarosides and a new pathway of biogenic amine metabolism in *Caenorhabditis elegans*. *J. Biol. Chem*. **288**, 18778–18783 (2013).
29. Pugin, B. et al. A wide diversity of bacteria from the human gut produces and degrades biogenic amines. *Microb. Ecol. Health Dis*. **28**, 1353881 (2017).
30. Barbieri, F., Montanari, C., Gardini, F. & Tabanelli, G. Biogenic amine production by lactic acid bacteria: a review. *Foods* **8**, 17 (2019).
31. Marcobal, A., Martín-Alvarez, P. J., Moreno-Arribas, M. V. & Muñoz, R. A multifactorial design for studying factors influencing growth and tyramine production of the lactic acid bacteria *Lactobacillus brevis* CECT 4669 and *Enterococcus faecium* BIFI-58. *Res. Microbiol*. **157**, 417–424 (2006).
32. Duerr, J. S. et al. The *cat-1* gene of *Caenorhabditis elegans* encodes a vesicular monoamine transporter required for specific monoamine-dependent behaviors. *J. Neurosci*. **19**, 72–84 (1999).
33. Sandmeier, E., Hale, T. I. & Christen, P. Multiple evolutionary origin of pyridoxal-5′-phosphate-dependent amino acid decarboxylases. *Eur. J. Biochem*. **221**, 997–1002 (1994).
34. Connil, N. et al. Identification of the *Enterococcus faecalis* tyrosine decarboxylase operon involved in tyramine production. *Appl. Environ. Microbiol*. **68**, 3537–3544 (2002).
35. Linares, D. M., Fernández, M., Martín, M. C. & Alvarez, M. A. Tyramine biosynthesis in *Enterococcus durans* is transcriptionally regulated by the extracellular pH and tyrosine concentration. *Microb. Biotechnol*. **2**, 625–633 (2009).
36. Zhu, H. et al. Crystal structure of tyrosine decarboxylase and identification of key residues involved in conformational swing and substrate binding. *Sci. Rep*. **6**, 27779 (2016).
37. Quick, M. et al. State-dependent conformations of the translocation pathway in the tyrosine transporter Tyt1, a novel neurotransmitter:sodium symporter from *Fusobacterium nucleatum*. *J. Biol. Chem*. **281**, 26444–26454 (2006).
38. Collins, K. M. et al. Activity of the *C. elegans* egg-laying behavior circuit is controlled by competing activation and feedback inhibition. *eLife* **5**, e21126 (2016).
39. Rex, E. et al. TYRA-2 (F01E11.5): a *Caenorhabditis elegans* tyramine receptor expressed in the MC and NSM pharyngeal neurons. *J. Neurochem*. **94**, 181–191 (2005).
40. Sun, J., Singh, V., Kajino-Sakamoto, R. & Aballay, A. Neuronal GPCR controls innate immunity by regulating noncanonical unfolded protein response genes. *Science* **332**, 729–732 (2011).
41. Elgaali, H. et al. Comparison of long-chain alcohols and other volatile compounds emitted from food-borne and related Gram positive and Gram negative bacteria. *J. Basic Microbiol*. **42**, 373–380 (2002).
42. Worthy, S. E. et al. Identification of attractive odorants released by preferred bacterial food found in the natural habitats of *C. elegans*. *PLoS ONE* **13**, e0201158 (2018).
43. Yoshida, K. et al. Odour concentration-dependent olfactory preference change in *C. elegans*. *Nat. Commun*. **3**, 739 (2012).
44. Zhang, F. et al. *Caenorhabditis elegans* as a model for microbiome research. *Front. Microbiol*. **8**, 485 (2017).
45. Leitão-Gonçalves, R. et al. Commensal bacteria and essential amino acids control food choice behavior and reproduction. *PLoS Biol*. **15**, e2000862 (2017).
46. Pais, I. S., Valente, R. S., Sporniak, M. & Teixeira, L. *Drosophila melanogaster* establishes a species-specific mutualistic interaction with stable gut-colonizing bacteria. *PLoS Biol*. **16**, e2005710 (2018).
47. Henriques, S. F. et al. Metabolic cross-feeding allows a gut microbial community to overcome detrimental diets and alter host behaviour. Preprint at https://www.biorxiv.org/content/10.1101/821892v1 (2019).
48. Breton, J. et al. Gut commensal *E. coli* proteins activate host satiety pathways following nutrient-induced bacterial growth. *Cell Metab*. **23**, 324–334 (2016).
49. Fetissov, S. O. Role of the gut microbiota in host appetite control: bacterial growth to animal feeding behaviour. *Nat. Rev. Endocrinol*. **13**, 11–25 (2017).

# Methods

No statistical methods were used to predetermine sample size. The experiments were not randomized and investigators were not blinded to allocation during experiments and outcome assessment.

### Strains

***C. elegans***. All *C. elegans* strains were maintained on NGM at 20 °C, and hermaphrodites were used for all experiments. *srv-11*p::*octr-1* (pMOD110) and *srg-47*p::*octr-1* (pMOD111) plasmids were injected at 10 ng/µl, *tbh-1*p::*tbh-1a*::*SL2*::*mcherry* (pMOD115) was injected at 20 ng/µl together with the *unc-122*p::*mcherry* co-injection marker at 30 ng/µl to generate transgenic strains. At least two independent lines were examined for all rescue experiments. Strain genotypes are listed in Supplementary Table 2.

**Bacteria.** For all experiments, bacterial strains were streaked from glycerol stocks before use and grown to saturation in LB medium at 37 °C. For conditioned medium, bacteria were grown to saturation in NGM medium overnight at 37 °C, then cleared by centrifugation at 14,000*g* for 3 min. Before use, conditioned medium or NGM was supplemented with 5× concentrated OP50 from a saturated LB culture to prevent starvation. To expose worms to bacterial odours, worms were grown on seeded NGM plates with lids that were replaced with NGM plates containing the test bacteria; these were sealed with parafilm. For L-Tyr and tyramine supplementation experiments, 0.5% (about 28 mM) L-Tyr (Sigma T3754), or 4 mM or 10 mM tyramine (Sigma T2879), were added to the NGM medium and agar before pouring plates. To generate antibiotic-killed bacteria, saturated cultures of OP50 or JUb39 were concentrated 5× by centrifugation followed by resuspension in LB medium containing 200 µg/ml gentamicin (Sigma G1397) for 4 h at 37 °C. Four 100-µl spots of these treated bacteria suspensions were added to 10-cm NGM plates and allowed to dry before adding L4-stage worms.

Plasmids were transformed into JUb39 and OP50 via electroporation. Deletions in JUb39 were induced using homologous recombination with the temperature-sensitive pSC101 replicon at 42 °C, and *sacB*-sucrose counter-selection at 30 °C, in the absence of NaCl as previously described[50], with the exception that bacteria were incubated for 1 h at room temperature in the presence of 10 mM arabinose for lambda Red induction before selection at 42 °C. Deletions were confirmed by sucrose resistance and kanamycin sensitivity, followed by PCR and sequencing of deleted intervals.

### Molecular biology

The *octr-1* cDNA was a gift from R. Komuniecki. The cDNA was amplified by PCR and cloned using Gibson homology cloning. The 1,940-bp *srv-11* promoter and 978-bp *srg-47* promoter sequences were cloned from genomic DNA. *tbh-1a* complementary (c)DNA was amplified from a mixed-stage cDNA pool by PCR. The 1,357-bp *tbh-1* promoter plasmid was a gift from M. Alkema. Vector maps are available on Github (https://github.com/SenguptaLab/ProvidenciaChemo.git). For introduction of deletions via homologous recombination in JUb39, pKD46-derivative plasmids containing a lambda Red cassette and deletion homology arms for JUb39 *tyrDC* and *adcA* were constructed (denoted pMOD102 and pMOD107, respectively). In brief, the *cas9* coding region and single-guide RNA regions of pDK46-derivative pCAS[51] were deleted and replaced with the *sacB* sequence from pCM433[52] via PCR and Gibson homology cloning. For pMOD102, 5′ and 3′ homology arms were approximately 400 bp each flanking a 1,233-bp deletion of the *tyrDC* coding sequence, which was replaced with a chloramphenicol resistance cassette. For pMOD107, 5′ and 3′ homology arms were 701 and 422 bp, respectively, flanking a 1,398-bp deletion of the *adcA* CDS. For expression of mCherry in OP50 and JUb39, a pUCP20T-mCherry plasmid[53] was modified to replace *bla*(ampR) with *aph*(kanR).

### Microscopy

All fluorescence and differential interference contrast microscopy was performed using worms anaesthetized with 100 mM levamisole (Sigma Aldrich). Worms were imaged on 2% agarose pads using an upright Zeiss Axio Imager with a 63× oil immersion objective.

**Quantification of intestinal bacterial cell numbers.** All rod-shaped punctae in the intestines of young adult worms of approximately 1–2 µm were included in the quantification. Each worm was recorded in one of three categories containing 0, <10 or >10 cells per worm. Exact numbers in worms with >10 cells were not recorded, but rarely exceeded approximately 100 cells.

**Fluorescence intensity measurements.** All images were collected in *z*-stacks of 0.5 µm through the heads of young adult worms. Quantification was performed using ImageJ (NIH). Fluorescence was quantified by identifying the focal plane in which the cell soma was visible, followed by manually drawing a region of interest around the soma. Mean pixel intensity was recorded for each neuron pair per worm and the average of fluorescence in each worm is shown.

### Quantification of intestinal colony-forming units

To estimate intestinal cell number, surface sterilization was performed as previously reported[54] with modifications. N2 young adult worms cultured for a single generation on OP50 or JUb39 were washed off a culture plate with M9 buffer, allowed to settle for 1–2 min followed by aspiration of supernatant. Worms were rinsed 4 more times with 1 ml M9 buffer, followed by one rinse with M9 + 25 mM levamisole (Sigma Aldrich) to block pharyngeal pumping. Worms were then incubated with 1% bleach in M9 + 25 mM levamisole for 5 min, followed by 5 more rinses with M9 buffer. One hundred microlitres of the final supernatant was plated on LB medium as a wash control. Worms were then placed on an NGM plate, after which 10 young adult worms per condition were picked into separate tubes containing 100 µl M9 buffer and were crushed using a pestle (UAS Scientific 1415-5390). The resulting samples were serially diluted and plated on LB medium. Colony-forming units per 10 worms were normalized by subtracting the number of colonies observed in plates from the wash control.

### *C. elegans* assays

**Long-range chemotaxis.** Long-range chemotaxis assays were performed essentially as previously described[8,55]. Worms were cultured for one generation with the relevant bacteria before the assay. Assays were performed using 10-cm square NGM plates. The number of worms in two horizontal rows adjacent to the odour and ethanol spots was quantified.

**SOS assays.** SOS assays in response to 1-octanol or 2-nonanone were performed as previously described[10,27]. NGM plates were predried for 1 h before assays. Age-matched young adult worms were picked from food to a clean transfer plate and allowed to briefly crawl away from food for approximately 1 min. Worms were then transferred to another clean NGM plate for 15 min before assaying responses to 100% octanol (Sigma O4500) and 100% 2-nonanone (Sigma 108731), or 20 min for 30% octanol assays. Thirty per cent octanol was prepared immediately before the assay by dilution in 200-proof ethanol (Acros Organics 61509-0010).

**Short-range bacterial choice assay.** Worms were raised and prepared identically to those used in long-range chemotaxis assays, with the exception that the final wash with water was omitted. NGM plates containing two 15-µl spots separated by 2 cm of overnight-grown bacterial food concentrated to an optical density at 600 nm of 10 were allowed to dry, then incubated with a closed lid for 5 h at room temperature.

Approximately 30 worms were placed between the two spots, and excess liquid was removed. Worms were allowed to navigate for 15 min, following which 2 µl of sodium azide was applied to each spot to anaesthetize worms. Minimal lawn-leaving behaviour was observed during this short time period. Adult worms on the control spot and test spot were counted.

**Osmotic avoidance assay.** Worms off the bacterial food on the cultivation plate were picked using a 10% methyl cellulose polymer solution and placed in the centre of an NGM plate with a ring of 8 M glycerol containing bromophenol blue (Sigma B0126). The number of worms inside and outside of the ring was counted after 10 min.

**Quantification of eggs in utero.** N2 or *tdc-1*-mutant worms were grown from egg to the L4 stage on NGM plates containing either OP50, JUb39 or *ΔtyrDC*::cmR *ΔadcA* JUb39. Age-matched L4 larvae were transferred to new plates 18 h before the assay. The number of eggs younger or older than the four-cell stage was recorded over three independent days of assays.

**Lifespan assays.** N2 worms were grown on 6-cm NGM plates containing 100 µl OP50, JUb39 or PA14. Twenty L4 worms were placed on each plate at the beginning of the experiment. Four replicate plates were analysed for each condition per day over three independent days of experiments. Worms were transferred to new plates at least once every two days until they ceased to lay eggs. Worms were censored if they crawled off of the plate, exhibited in utero larval hatching ('bagging') or if they were injured during transfers. Worms were scored as dead if they did not respond to being prodded in the head.

**Tyrosine supplement for metabolomics assay.** *tdc-1*-mutant worms were grown on plates containing 0.5% L-Tyr (w/v) or at the same concentration containing a 1:1 mixture of L-Tyr and 3,3-$d_2$-L-Tyr, purchased from Cambridge Isotope Laboratories (DLM-2317-.5).

### Bacteria genome sequencing

Sequencing was performed by the Broad Technology Labs at the Broad Institute. Resulting PacBio reads for JUb39 and PYb007 were assembled using Canu v.1.8 (https://github.com/marbl/canu.git)[56]. Assemblies were trimmed, oriented and circularized using Circlator v.1.5.5 (https://sanger-pathogens.github.io/circlator/)[57].

### Phylogenetic analysis of genes encoding group-II pyridoxal-dependent decarboxylases

JUb39 TyrDC and AdcA were initially identified as the only significant (*E*-value $4 \times 10^{-149}$ and $3 \times 10^{-12}$, respectively) hits via a tblastn search of the draft JUb39 genome assembly using *Enterococcus faecalis* TyrDC as a query sequence. An initial BLASTP screen of the nr sequence database restricted to bacteria was performed using the *P. alcalifaciens* J Ub39 TyrDC and AdcA putative coding regions. Searches were performed hierarchically; limited initially to Enterobacteriaceae, followed by Enterobacterales, Gammaproteobacteria, Proteobacteria and finally all Eubacteria. With the exception of members of Morganellaceae (*Providencia*, *Proteus*, *Morganella*, *Xenorhabdus*, *Photorhabdus*, *Arsenophonus* and *Moellerella*), only two protein sequences per genus were retained for subsequent phylogenetic analysis. Representative group-II decarboxylase enzymes with known substrate specificity from Eukaryota and Archaea, as well as glutamate decarboxylase (encoded by *gadA* and *gadB*) and histidine decarboxylase sequences, were also included.

Multiple sequence alignments were produced using the Phylomizer workflow (https://github.com/Gabaldonlab/phylomizer), which used the MUSCLE v.3.8.31 (http://www.drive5.com/muscle)[58], MAFFT v.7.407 (https://mafft.cbrc.jp/alignment/software)[59] and Kalign v.2.04 (http://msa.sbc.su.se/cgi-bin/msa.cgi)[60] multiple sequence aligners; these were trimmed to produce a consensus alignment using trimAL v.1.4rev15 (https://github.com/scapella/trimal)[61]. An initial phylogenetic tree was produced using PhyML v.3.3.20180621 (http://www.atgc-montpellier.fr/phyml/)[62] using the NNI algorithm with an LG substitution model. This tree showed three major, well-supported clusters containing: (1) *Enterococcus* and *Providencia* TyrDC (denoted '*Enterococcus*-type TDC'); (2) eukaryotic and bacterial AADCs (denoted 'Eukaryotic-type AADC'); and (3) *Morganella* AdcA and *Providencia* AdcA.

On the basis of this initial tree, a second tblastn search was used to determine the presence or absence of homologous genes among complete Gammaproteobacteria genomes. *Enterococcus faecalis* TyrDC and *C. elegans* TDC-1 were used as tblastn search query sequences. A hierarchical search was performed as described, limited to an *e*-value cutoff of $10^{-5}$. A maximum of two highly similar sequences were retained per genus for phylogenetic analysis, as listed in Supplementary Table 1.

A final phylogenetic tree was constructed using the amino acid sequences derived from these tblastn queries. These sequences were assembled into a consensus alignment using the Phylomizer workflow as described. ProtTest (https://github.com/ddarriba/prottest3)[63] was used to identify the optimal model for likelihood estimation, using Aikake information criterion values for selection. The model selected and subject to PhyML analysis was an LG model with discrete gamma distribution, an estimated proportion of invariant sites (+I), empirical frequencies of amino acids (+F), estimated gamma shape parameter (+G) for rate variation among sites with the default four substitution-rate categories, and the subtree pruning and regrafting (SPR) algorithm. One hundred bootstrap pseudoreplicates were analysed. Representatives from the resulting phylogeny were used to categorize and compile the cladogram in Fig. 3b. Adjacent genomic sequences, up to three CDS 5′ or 3′, were examined for genes that encode amino acid permeases or transporters in an apparent operon as defined by close proximity and same orientation with respect to each tblastn hit (Supplementary Table 1).

### Molecular modelling

The putative amino acid sequence for the JUb39 TyrDC was used to model active site residues using the *Lactobacillus* TyrDC crystal structure in complex with pyridoxyl phosphate (Protein Data Bank code 5HSJ.1[36]) as a template guide using SWISS-MODEL (https://swissmodel.expasy.org)[64]. This resulted in a Qmean *z*-score of 0.33, indicative of good agreement between structures. This process was also attempted with AdcA, and modelling was performed with the top six available structures on the basis of sequence homology. The maximum QMean of AdcA was found with *Lactobacillus* TyrDC, but with a value −5.71, indicative of low quality. Resulting models were visualized using Chimera v.1.13.1 (https://www.cgl.ucsf.edu/chimera/)[65]. For Extended Data Fig. 8d, L-Tyr was manually docked according to the reported docking position[36] for illustrative purposes only.

### Statistical analyses

All statistical analyses were performed in R (https://www.R-project.org/)[66] and RStudio (http://www.rstudio.com)[67]. Sample sizes were chosen according to conventional estimates of power for all assays. No randomization or blinding was performed. For modulation index and relative latency figures, data were normalized to the relevant control-group mean value for each experimental day on the log scale via subtraction. Outliers in box plots were defined as greater than 1.5× interquartile range, but were included for analysis. All statistical analyses were performed on raw, non-normalized data. To avoid inflated *P* values and to account for nonindependence of observations, we used mixed-effects regression analysis in lieu of simple analysis of variance (ANOVA) and *t*-tests. For behavioural assays, frequentist statistical comparisons were performed using a binomial GLMM with a logit link function for chemotaxis, food choice and egg-in-utero assays, and an LMM on $\log_{10}$-transformed data was used to analyse SOS assays using the 'lme4' package v.1.1-21[68]. In all cases, a random intercept term for

assay plate was used to account for non-independence of worms on each assay plate and a random intercept for date was used to account for day-to-day variability. In the presence of interactions (for example, the effects of bacterial strains across different odorants in Fig. 1a and Extended Data Fig. 1a), a random slope term per date was also used when appropriate. Estimated *P* values for pairwise comparison of fixed effects were determined using Kenward–Roger approximated degrees of freedom as implemented in the emmeans v.1.4.5[69] and pbkrtest v.0.4-86[70] packages. In nearly all cases, inclusion of random effects model terms resulted in conservative *P* value estimates compared to a simple ANOVA. Post hoc corrections for multiple comparisons and type-I error were implemented using the emmeans package. In the event of singular model fit, any random slope term followed by random date effect terms were removed to allow convergence. For Wald statistics of model terms, the package lmerTest v.3.1-1[71] or car v.3.0-6[72] was used.

Additionally, for each dataset, a maximal Bayesian model was fit using the rstanarm v.2.19.3[73] package. Data presented are posterior credible intervals for fixed effect levels derived from posterior fitted values of the Markov chain Monte Carlo chains as implemented by the emmeans, coda v.0.19-3[74], bayesplot v.1.7.1[75] and tidybayes v.2.0.1[76] packages. For comparison of intestinal bacterial cell numbers, an ordinal logistic regression was performed using the MASS v.7.3-51.4[77] package and polr function. Categories of cell numbers were considered ordered factors of none, some or many cells.

For survival analysis, data were fit to a Gompertz–Makeham function using the nls function in R using the following equation: $S(t) = e^{\wedge}(-(G/\gamma) \times (e^{\wedge}(\gamma t) - 1))$. Bootstrap confidence intervals were derived from 1,000 bootstrap samples with replacement, followed by nls fit. To calculate bootstrap median survival, using each nls fit and solving for $t$ at $S = 0.5$ yielded the equation: $t = (1/\gamma) \times \ln(1 - (\gamma/G) \times \ln(0.5))$.

### Sample preparation for HPLC–MS

Approximately 10,000 mixed-staged worms in 1.5-ml microfuge tubes were lyophilized for 18–24 h using a VirTis BenchTop 4K Freeze Dryer. After the addition of 2 stainless steel grinding balls and 1 ml of 80% methanol, samples were sonicated for 5 min (2 s on/off pulse cycle at 90 A) using a Qsonica Q700 Ultrasonic Processor with a water bath cup horn adaptor (model 431C2). Following sonication, microfuge tubes were centrifuged at 10,000 RCF for 5 min in an Eppendorf 5417R centrifuge. Eight hundred microlitres of the resulting supernatant was transferred to a clean 4-ml glass vial, and 800 µl of fresh methanol added to the sample. The sample pellet was again sonicated and centrifuged, and the two supernatants were combined and concentrated to dryness in an SC250EXP Speedvac Concentrator coupled to an RVT5105 Refrigerated Vapour Trap (Thermo Scientific). The resulting powder was suspended in 120 µl of 100% methanol, followed by vigorous vortex and brief sonication. This solution was transferred to a clean microfuge tube and subjected to centrifugation at 20,000 RCF for 10 min in an Eppendorf 5417R centrifuge to remove precipitate. The resulting supernatant was transferred to an HPLC vial and analysed by HPLC–MS.

### HPLC–MS analyses

Reversed-phase chromatography was performed using a Vanquish LC system controlled by Chromeleon Software (Thermo Fisher Scientific) and coupled to an Orbitrap Q-Exactive High Field mass spectrometer controlled by Xcalibur software (Thermo Fisher Scientific). Methanolic extracts prepared as described in 'Sample preparation for HPLC–MS' were separated on an Agilent Zorbax Eclipse XDB-C18 column (150 mm × 2.1 mm, particle size 1.8 µm) maintained at 40 °C with a flow rate of 0.5 ml/min. Solvent A: 0.1% formic acid in water; solvent B: 0.1% formic acid in acetonitrile. A–B gradient started at 5% B for 3 min after injection and increased linearly to 98% B at 20 min, followed by 5 min at 98% B, then back to 5% B over 0.1 min and finally held at 5% B for an additional 2.9 min to re-equilibrate the column. Mass spectrometer parameters were: spray voltage, −2.9 kV/+3.5 kV; capillary temperature 380 °C; probe heater temperature 400 °C; sheath, auxiliary and sweep gas, 60, 20 and 2 AU, respectively; S-Lens RF level, 50, resolution 240,000 at $m/z$ 200; AGC target, $3 \times 10^6$. Each sample was analysed in negative (ESI−) and positive (ESI+) electrospray ionization modes with $m/z$ range 150–800. Parameters for tandem mass spectrometry (MS/MS) (dd-MS2): MS1 resolution, 60,000; AGC target, $1 \times 10^6$. MS2 resolution, 30,000; AGC target, $2 \times 10^5$; maximum injection time, 50 msec; isolation window, 1.0 $m/z$; stepped normalized collision energy (NCE), 10, 30; dynamic exclusion, 5 s; top 10 masses selected for MS/MS per scan. LC–MS data were analysed using Metaboseek software (as described in 'Metabolic network analysis') and quantification performed via integration in Excalibur Quan Browser (Thermo Fisher Scientific).

### Metabolic network analysis

We performed MS2 networking using Metaboseek MS analysis software (https://doi.org/10.5281/zenodo.3360087)[78]. Documentation and source code are available in the Metaboseek R package on GitHub: https://github.com/mjhelf/Metaboseek. Additional information, installation instructions and a user guide are available at https://metaboseek.com. The xcms package[79] within Metaboseek was used with 'Metaboseek_default' settings, suitable for high-resolution mass spectrometry instruments, followed by MS2 matching using the following parameters: ppm window, 3; RT window, 5 s; 'unique assignments' on. From roughly 200,000 features detected in ESI+ HPLC–MS, approximately 10,000 features were matched to MS2 spectra, which was further culled to 4,563 features using the 'Peak Shapes' functionality to calculate peak quality scores, applying a threshold of 0.97. Networking was performed using the Compare MS2 function in Metaboseek with the following parameters: $m/z$ tolerance, 0.002; ppm tolerance, 3; min. number of peaks in common, 4; noise level, 2%; with 'parent masses' turned on and 'ignore small fragments' ($m/z < 100$) turned on. The network was modified by removing edges below similarity score (cosine) = 0.7, and further simplified by restricting the maximum number of edges per node to the top 5 ranked by similarity score.

### Reporting summary

Further information on research design is available in the Nature Research Reporting Summary linked to this paper.

## Data availability

All data necessary to reproduce these analyses are available as Source Data and/or at https://github.com/SenguptaLab/ProvidenciaChemo.git. Raw data from HPLC–MS experiments are available upon request (owing to the large file sizes).

## Code availability

All statistical analysis code necessary to reproduce these analyses are available at https://github.com/SenguptaLab/ProvidenciaChemo.git.


50. Blomfield, I. C., Vaughn, V., Rest, R. F. & Eisenstein, B. I. Allelic exchange in *Escherichia coli* using the *Bacillus subtilis sacB* gene and a temperature-sensitive pSC101 replicon. *Mol. Microbiol.* **5**, 1447–1457 (1991).
51. Jiang, Y. et al. Multigene editing in the *Escherichia coli* genome via the CRISPR–Cas9 system. *Appl. Environ. Microbiol.* **81**, 2506–2514 (2015).
52. Marx, C. J. Development of a broad-host-range sacB-based vector for unmarked allelic exchange. *BMC Res. Notes* **1**, 1 (2008).
53. Barbier, M. & Damron, F. H. Rainbow vectors for broad-range bacterial fluorescence labeling. *PLoS ONE* **11**, e0146827 (2016).
54. Alegado, R. A. & Tan, M.-W. Resistance to antimicrobial peptides contributes to persistence of *Salmonella typhimurium* in the *C. elegans* intestine. *Cell. Microbiol.* **10**, 1259–1273 (2008).
55. Troemel, E. R., Kimmel, B. E. & Bargmann, C. I. Reprogramming chemotaxis responses: sensory neurons define olfactory preferences in *C. elegans*. *Cell* **91**, 161–169 (1997).
56. Koren, S. et al. Canu: scalable and accurate long-read assembly via adaptive *k*-mer weighting and repeat separation. *Genome Res.* **27**, 722–736 (2017).
57. Hunt, M. et al. Circlator: automated circularization of genome assemblies using long sequencing reads. *Genome Biol.* **16**, 294 (2015).

58. Edgar, R. C. MUSCLE: multiple sequence alignment with high accuracy and high throughput. *Nucleic Acids Res*. **32**, 1792–1797 (2004).
59. Katoh, K., Misawa, K., Kuma, K. & Miyata, T. MAFFT: a novel method for rapid multiple sequence alignment based on fast Fourier transform. *Nucleic Acids Res*. **30**, 3059–3066 (2002).
60. Lassmann, T. & Sonnhammer, E. L. L. Kalign—an accurate and fast multiple sequence alignment algorithm. *BMC Bioinformatics* **6**, 298 (2005).
61. Capella-Gutiérrez, S., Silla-Martínez, J. M. & Gabaldón, T. trimAl: a tool for automated alignment trimming in large-scale phylogenetic analyses. *Bioinformatics* **25**, 1972–1973 (2009).
62. Guindon, S. et al. New algorithms and methods to estimate maximum-likelihood phylogenies: assessing the performance of PhyML 3.0. *Syst. Biol*. **59**, 307–321 (2010).
63. Darriba, D., Taboada, G. L., Doallo, R. & Posada, D. ProtTest 3: fast selection of best-fit models of protein evolution. *Bioinformatics* **27**, 1164–1165 (2011).
64. Waterhouse, A. et al. SWISS-MODEL: homology modelling of protein structures and complexes. *Nucleic Acids Res*. **46**, W296–W303 (2018).
65. Pettersen, E. F. et al. UCSF Chimera—a visualization system for exploratory research and analysis. *J. Comput. Chem*. **25**, 1605–1612 (2004).
66. R Core Team. R: A language and environment for statistical computing (R Foundation for Statistical Computing, 2019).
67. RStudio Team. RStudio: integrated development for R (RStudio, 2019).
68. Bates, D., Maechler, M., Bolker, B. & Walker, S. Fitting linear mixed-effects models using lme4. *J. Stat. Softw*. **67**, 1–48 (2015).
69. Lenth, R. emmeans: estimated marginal means, aka least-squares means. R package v.1.4.5, https://CRAN.R-project.org/package=emmeans (2020).
70. Halekoh, U. & Højsgaard, S. A Kenward–Roger approximation and parametric bootstrap methods for tests in linear mixed models – the R package pbkrtest. *J. Stat. Softw*. **59**, 1–30 (2014).
71. Kuznetsova, A., Brockhoff, P. B. & Christensen, R. H. B. lmerTest package: tests in linear mixed effects models. *J. Stat. Softw*. **82**, 1–26 (2017).
72. Fox, J. & Weisberg, S. *An R Companion to Applied Regression* 3rd edn (Sage, 2019).
73. Goodrich, B., Gabry, J., Ali, I. & Brilleman, S. rstanarm: Bayesian applied regression modeling via Stan, https://mc-stan.org/rstanarm (2020).
74. Plummer, M., Best, N., Cowles, K. & Vines, K. CODA: convergence diagnosis and output analysis for MCMC. *R News* **6**, 7–11 (2006).
75. Gabry, J., Simpson, D., Vehtari, A., Betancourt, M. & Gelman, A. Visualization in Bayesian workflow. *J. R. Stat. Soc. A*. **182**, 389–402 (2019).
76. Kay, M. tidybayes: tidy data and geoms for Bayesian models, https://doi.org/10.5281/zenodo.1308151 (2020).
77. Venables, W. N. & Ripley, B. D. *Modern Applied Statistics with S* 4th edn (Springer, 2002).
78. Helf, M. Metaboseek: an interactive, browser-based tool to analyze your mass spectrometry data, https://doi.org/10.5281/zenodo.3360087 (2019).
79. Smith, C. A., Want, E. J., O'Maille, G., Abagyan, R. & Siuzdak, G. XCMS: processing mass spectrometry data for metabolite profiling using nonlinear peak alignment, matching, and identification. *Anal. Chem*. **78**, 779–787 (2006).



**Acknowledgements** We thank R. Komuniecki for the *octr-1* cDNA; M. Alkema for the *tbh-1* promoter; multiple members of the *C. elegans* community for bacterial strains (listed in Supplementary Table 2); the *Caenorhabditis* Genetics Center for *C. elegans* strains; the Broad Institute for bacterial genome sequencing; M. Helf for assistance with the Metaboseek software; J. Yu and H. Le for synthesis of *N*-succinyl neurotransmitter standards; S. Lovett, L. Laranjo, M. Alkema and the laboratory of P.S. for advice; and C. Bargmann, O. Hobert and the laboratory of P.S. for comments on the manuscript. This work was partly supported by the NIH (T32 NS007292 and F32 DC013711 to M.P.O.; R01 GM088290 and R35 GM131877 to F.C.S.; and R35 GM122463 and R21 NS101702 to P.S.) and the NSF (IOS 1655118 to P.S.).


**Author contributions** M.P.O., B.W.F., F.C.S. and P.S. designed experiments, interpreted results and wrote the paper with input from all authors. M.P.O. and P.-H.C. conducted long-range chemotaxis behavioural experiments and analysed results. B.W.F. conducted HPLC–MS experiments and analysed results. M.P.O. conducted and analysed results from all additional experiments.

**Competing interests** The authors declare no competing interests.

**Additional information**


**Supplementary information** is available for this paper at https://doi.org/10.1038/s41586-020-2395-5.



**Correspondence and requests for materials** should be addressed to M.P.O. or P.S.



**Peer review information** *Nature* thanks William Schafer and the other, anonymous, reviewer(s) for their contribution to the peer review of this work.

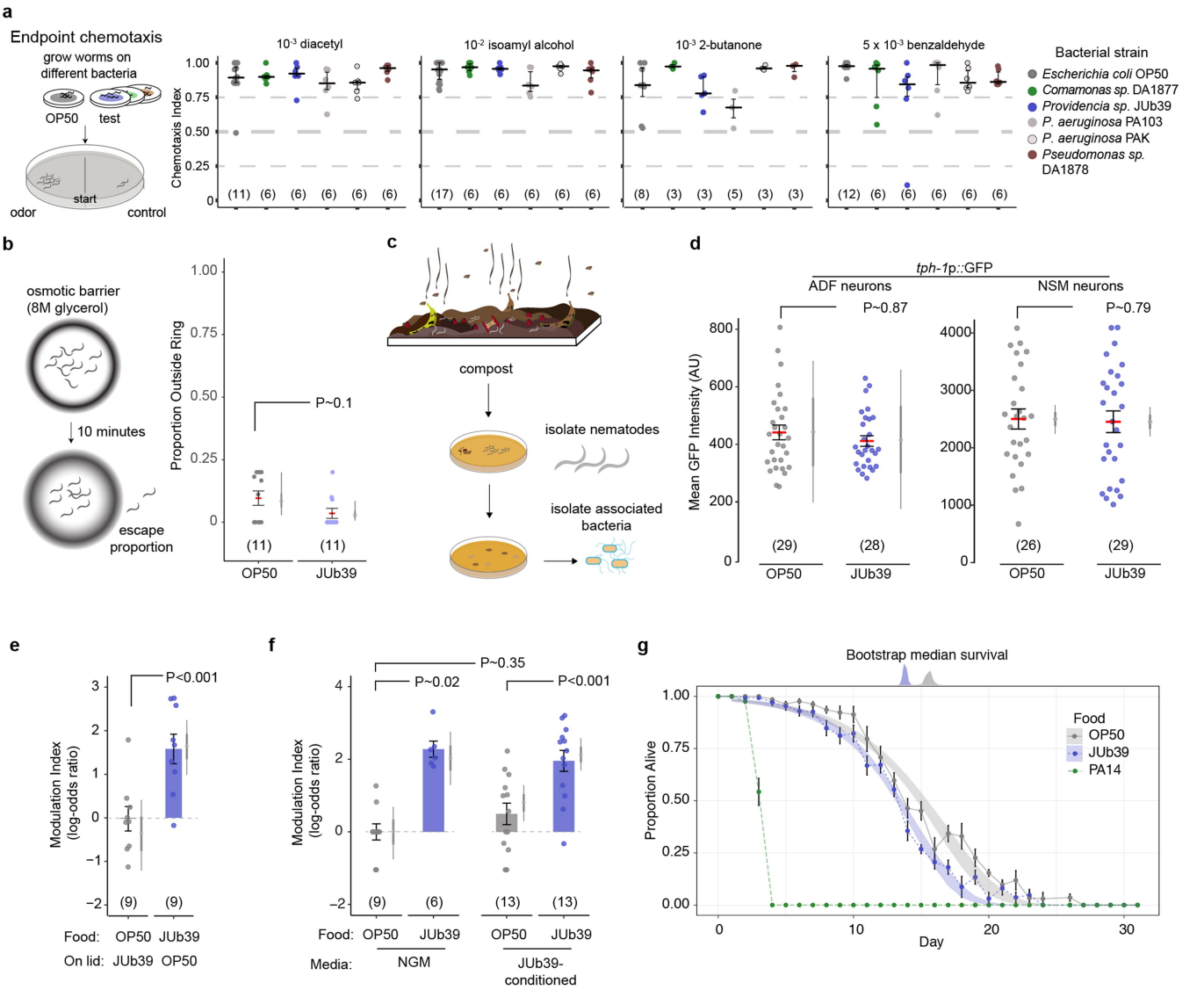


**Extended Data Fig. 1 | Octanol modulation by *Providencia* requires ingestion of bacteria and is not mediated by nutritive cues. a**, Cartoon and data from long-range chemotaxis assays of *C. elegans* grown on the indicated bacterial strains to the indicated attractive odours. Dots, chemotaxis index from single assays of approximately 100 worms. Horizontal line, median; errors, 1st and 3rd quartiles. Numbers in parentheses, number of assays performed over at least three days. **b**, Cartoon and data from osmotic ring avoidance assay. Dots, single assays of 10 worms. Numbers in parentheses, number of assays over at least three independent days. *Y* axis is the proportion of worms leaving an osmotic ring barrier of 8 M glycerol after 10 min. *P* value represents difference of means relative to worms grown on JUb39 from a GLMM. Errors are s.e.m. Grey thin and thick vertical bars, Bayesian 95% and 66% credible intervals, respectively. **c**, Isolation of nematode-associated bacteria. Nematodes were isolated from residential compost in Massachusetts (USA). Worms were allowed to crawl onto NGM plates from which they were picked to clean plates. Resulting bacterial colonies were isolated, grown on LB medium and characterized via 16S rRNA sequencing. **d**, Expression of a *tph-1*p::*gfp* fluorescent reporter in indicated head neurons of young adult worms grown on either OP50 or JUb39. Dots, mean fluorescence of the soma of single neurons. Horizontal bar is mean; errors are s.e.m. Grey thin and thick vertical bars, Bayesian 95% and 66% credible intervals, respectively. *P* values are from two-way ANOVA. **e**, **f**, Modulation index of worms grown on the indicated bacterial strains to 100% octanol, under the shown conditions. Worms were exposed to the indicated bacteria on the plate lid (**e**) for one generation, or to NGM control or bacteria-conditioned NGM (**f**) for 2 h before the assay. Numbers in parentheses, independent experiments over 2 d with approximately 100 worms each. Values are shown on a log-odds (logit) scale and are normalized to the values of wild-type worms grown on OP50 for each day, indicated with a grey dashed line. Positive numbers indicate reduced avoidance of octanol. Errors are s.e.m. Grey thin and thick vertical bars, Bayesian 95% and 66% credible intervals, respectively. *P* values between the indicated conditions are post hoc comparisons from a GLMM, with Tukey-type multivariate *t* adjustment for **f**. **g**, Survival analysis of worms grown on the indicated strains. Dots, average proportion of surviving worms from 12 plates of 20 worms each on the indicated days. Error bars are s.e.m. Shaded blue and grey curves indicate 95% confidence intervals derived from 1,000 bootstrap Gompertz function nonlinear least squares (nls) fits of the indicated data. Top blue and grey distributions show bootstrapped median survival of the indicated strains.

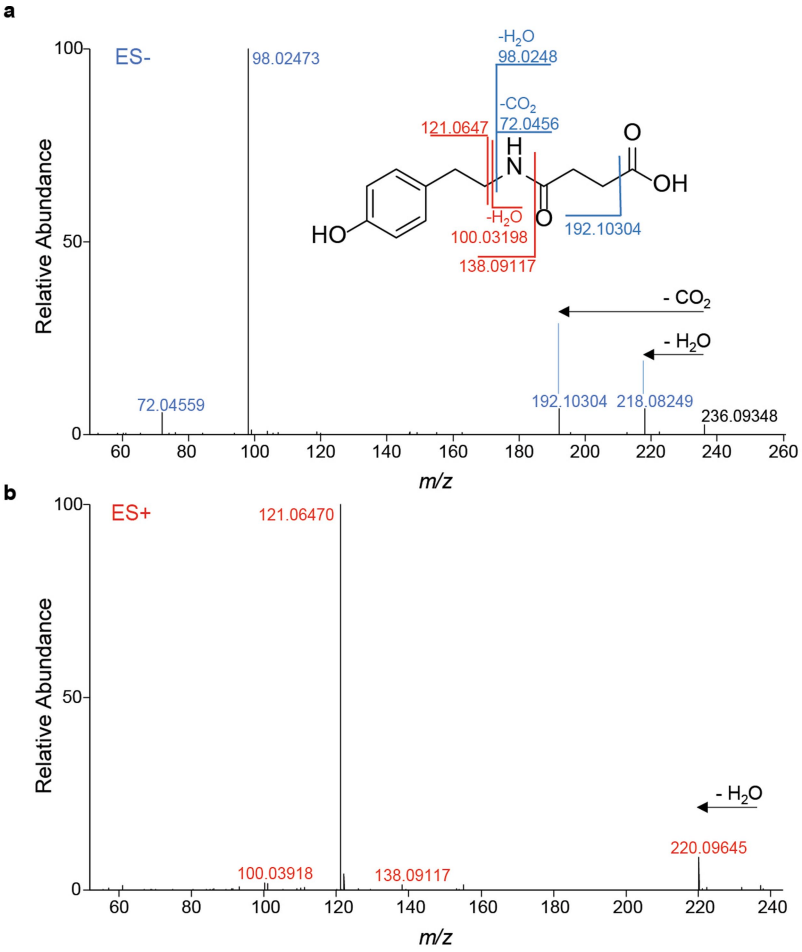


**Extended Data Fig. 2 | Detection of *N*-succinyl tyramine. a**, **b**, Major fragmentation reactions and resulting fragment ions are indicated in mass spectra of *N*-succinyl tyramine obtained in ESI− (**a**) and ESI+ (**b**) HPLC–MS2. Representative data are shown from at least three biologically independent experiments.

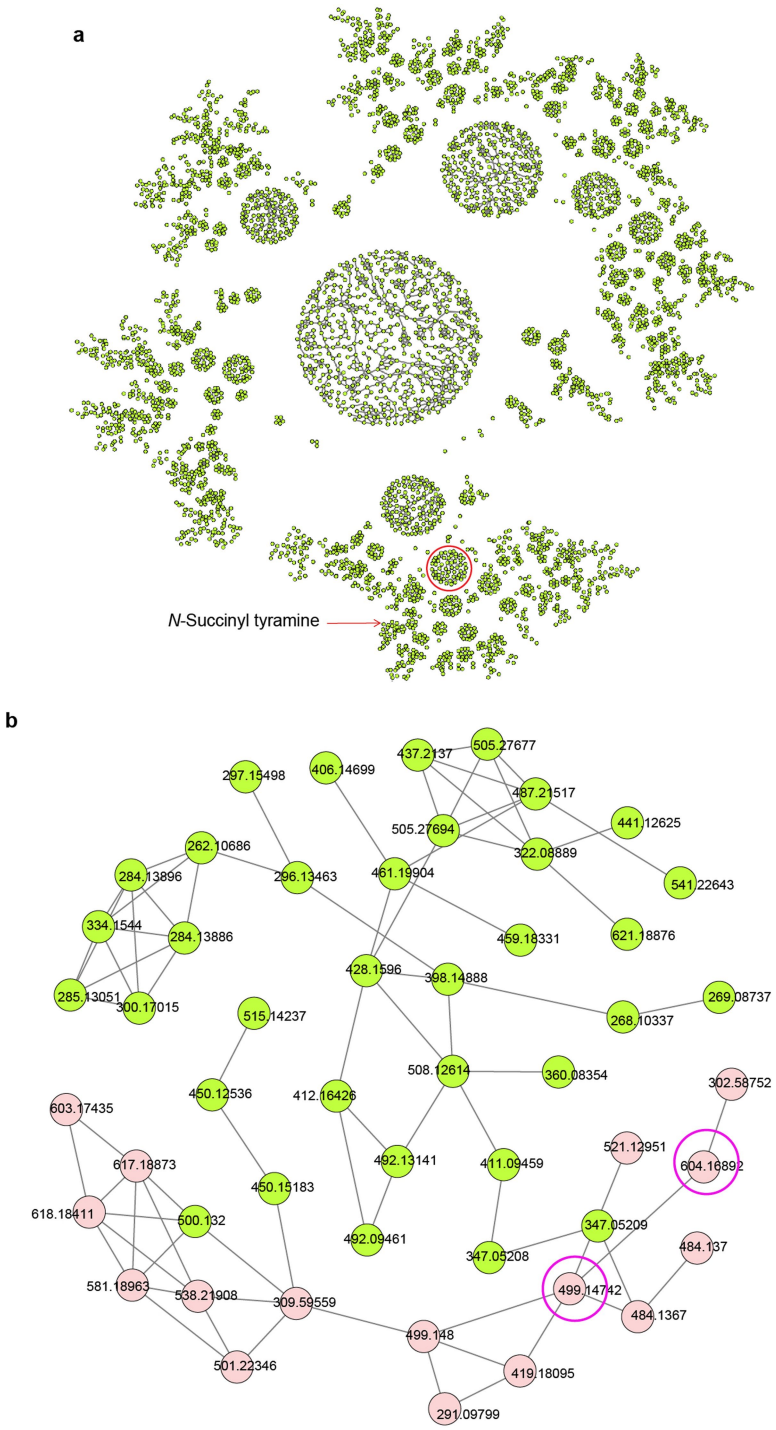


**Extended Data Fig. 3 | Complementation of tyramine-containing metabolites in *tdc-1*-mutant worms via *Providencia* AADCs. a**, Overview of MS2 network obtained in positive ion mode. Each node represents a unique feature, and edges between nodes indicate similarity between MS2 spectra. Red circle highlights the subnetwork containing the majority (16 out of 24 features, representing 10 out of 15 differential compounds) of differential tyramine-containing metabolites. This subnetwork contains glycosylated tyramine derivatives; *N*-succinyl tyramine is represented by a node in a different sub-network (red arrow). **b**, Magnified view of subnetwork highlighted in **a**. The tyramine-containing features restored upon growth of *tdc-1*-mutant worms on wild-type JUb39, and abolished when grown on *ΔtyrDC*::cmR *ΔadcA* JUb39, are highlighted in light red. MS2 spectra for two example compounds at *m/z* 499.1474 and *m/z* 604.1689 (circled in magenta) are shown in Extended Data Figs. 4 and 5, respectively.

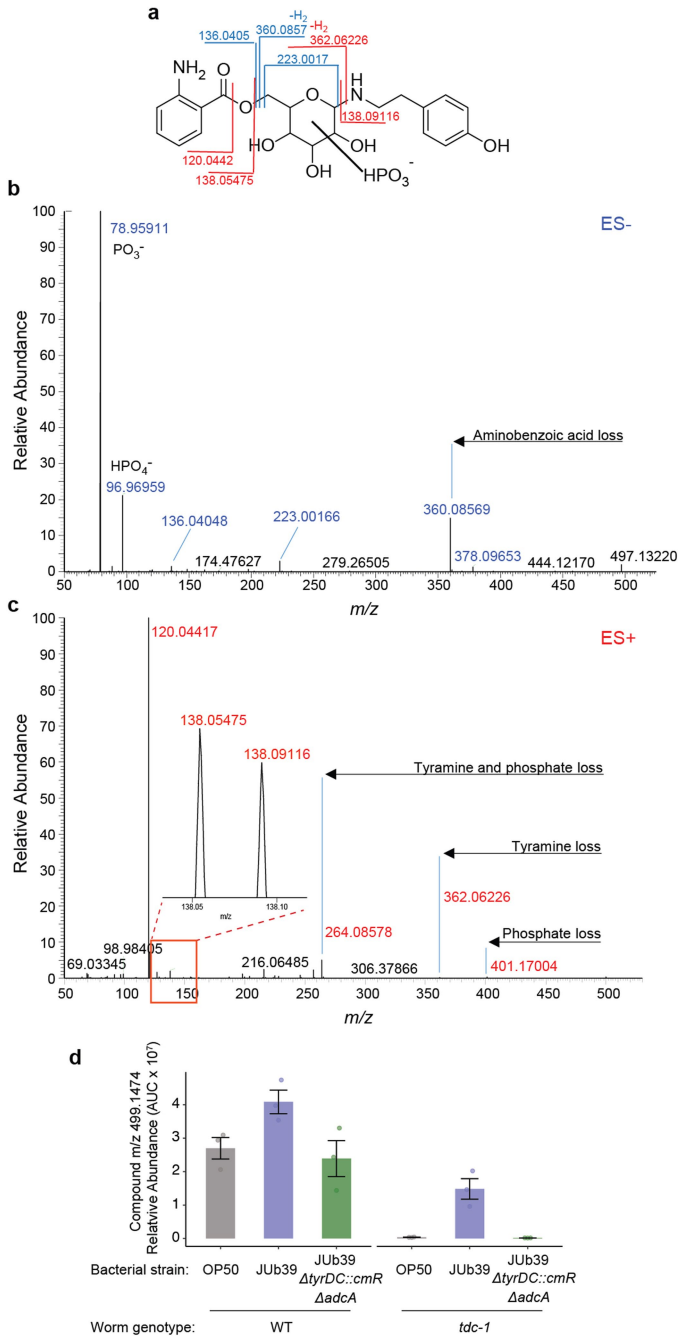


**Extended Data Fig. 4 | MS2 analysis and quantification of the tyramine-containing metabolite *m/z* 499.1474. a**, Major fragmentation reactions of *m/z* 499.1474 and resulting fragment ions. The putative structure shown is based on fragmentation and stable-isotope incorporation. The stereochemistry and exact substitution pattern are unknown. **b**, **c**, MS2 spectra obtained in ESI− (**b**) and ESI+ (**c**) mode. Representative data are shown from at least three biologically independent experiments. **d**, Quantification of *m/z* 499.1474 in wild-type and *tdc-1*-mutant worms fed the indicated bacterial strains as determined by positive-ion ESI+ HPLC–MS. Dots, independent samples from $n = 3$ experiments. Errors are s.e.m.

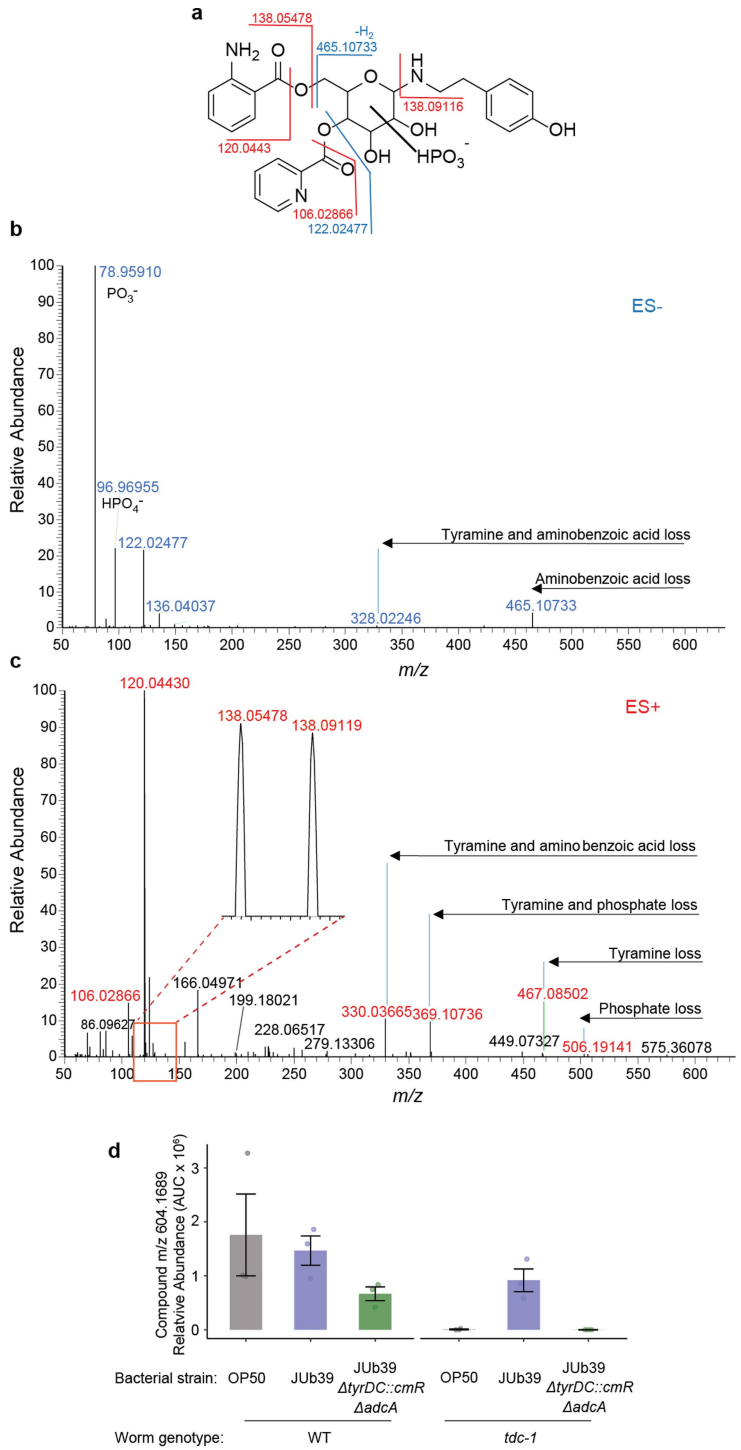


**Extended Data Fig. 5 | MS2 analysis and quantification of the tyramine-containing metabolite *m/z* 604.1689. a**, Major fragmentation reactions of *m/z* 604.1689 and resulting fragment ions. The stereochemistry and exact substitution pattern are unknown. The structure shown is based on fragmentation and stable-isotope incorporation. **b**, **c**, MS2 spectra obtained in negative-ion (**b**) and positive-ion (**c**) mode. Representative data are shown from at least three biologically independent experiments. **d**, Quantification of *m/z* 604.1689 in wild-type and *tdc-1*-mutant worms fed the indicated bacterial strains as determined by positive-ion ESI HPLC–MS. Dots, independent samples from $n = 3$ experiments. Errors are s.e.m.

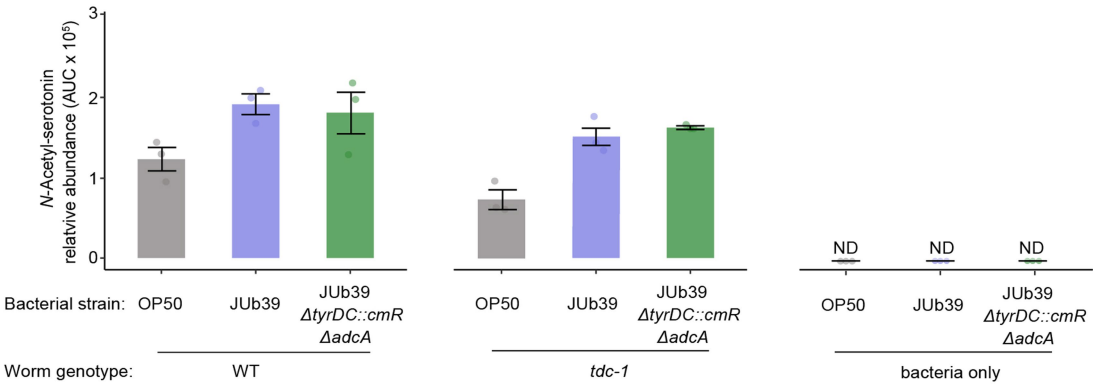


**Extended Data Fig. 6 | Quantification of *N*-acetyl serotonin in worms fed the indicated bacteria, or in bacterial cultures alone, as determined by ESI+ HPLC–MS.** Dots, independent samples from $n = 3$ experiments. Errors are s.e.m.

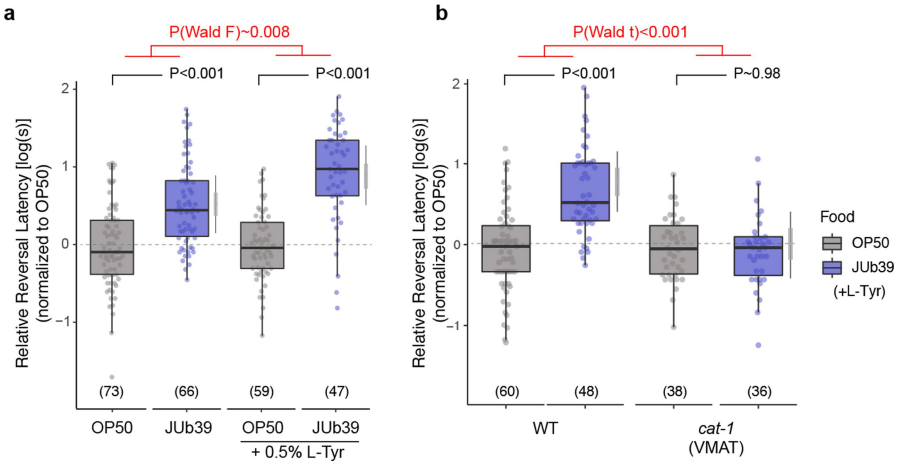


**Extended Data Fig. 7 | L-Tyr supplementation enhances octanol modulation. a**, **b**, Reversal response times of worms of the indicated genotypes grown on the indicated bacteria in control conditions (**a**) or supplemented with 0.5% L-Tyr (**a**, **b**) to 100% octanol using SOS assays. Dots, response time of single worms. *Y* axis is $\log_{10}$-scaled for these log-normally distributed data, and normalized to the indicated control group for each experimental day. Numbers in parentheses, number of worms tested in assays over at least three independent days. Box plot, median and quartiles; whiskers, data range (excluding outliers). Grey thin and thick vertical bars, Bayesian 95% and 66% credible intervals for the difference of means, respectively. *P* values indicating comparisons of means relative to the OP50 control for each of the conditions are from an LMM with Tukey-type multivariate *t* adjustment. *P* value in red indicates Wald *F*-statistic (**a**) or Wald *t*-statistic (**b**) for the effect of L-Tyr supplementation (**a**) or genotype (**b**) on the magnitude of the JUb39 effect. Wild-type data in **b** are also shown in Fig. 2g.

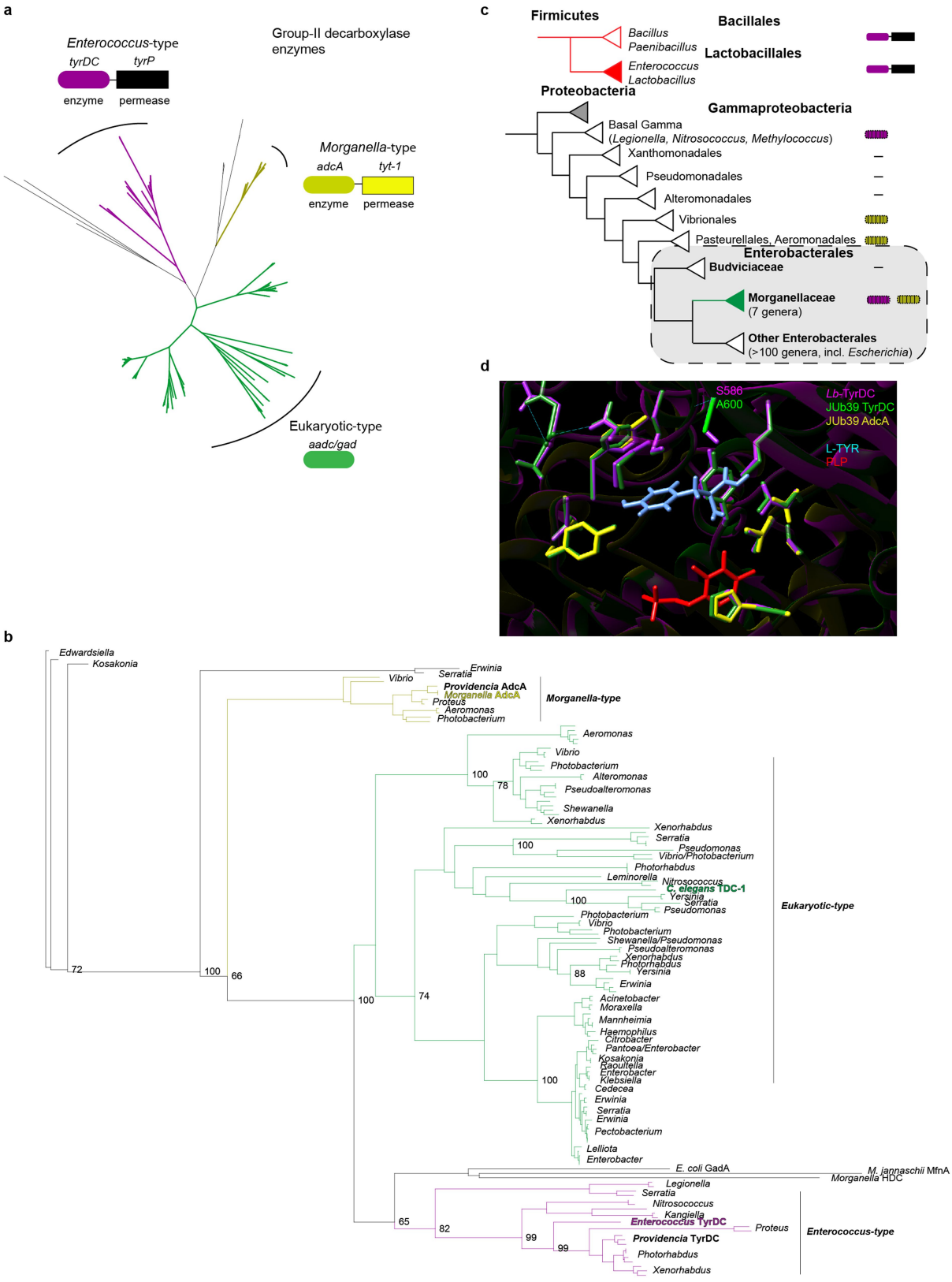


**Extended Data Fig. 8** | See next page for caption.

**Extended Data Fig. 8 | Phylogenetic analysis of group-II decarboxylase genes in Gammaproteobacteria. a**, Neighbour-joining unrooted tree based on sequences identified via a BLAST search using *E. faecalis* TyrDC and *C. elegans* TDC-1. The initial tree indicates three major groups. Representative enzymes and operon structures for each group are indicated by coloured boxes. **b**, Bootstrapped maximum likelihood phylogeny using PhyML and Phylomizer pipeline. Maximum of two highly similar sequences per genus were included after each BLAST search. Genera are indicated to the right. Numbers on branch-points matching this tree out of 100 bootstrap replicates are indicated at values >60. Group representatives from **a** are indicated in corresponding colours. *Providencia* and *C. elegans* sequences discussed in this Article are indicated in bold. Accession numbers and BLAST metrics are listed in Supplementary Table 1. **c**, Presence of *tyrDC* and *adcA* among complete genomes in Gammaproteobacteria. Linked boxes indicate organization in an operon. Hatched shading indicates variable presence among genera. Coloured triangles indicate taxa of interest. **d**, Homology-based model of the TyrDC catalytic domain in *Providencia* based on the *Lactobacillus* TyrDC crystal structure[36] using SWISS-MODEL (https://swissmodel.expasy.org). Residues in magenta, green and yellow are from *Lactobacillus* TyrDC, JUb39 TyrDC and JUb39 AdcA, respectively. Pyridoxyl phosphate (PLP) is depicted in red and L-Tyr (manually docked for illustration) is indicated in light blue. Position of A600 and S586[36] in JUb39 TyrDC and *Lactobacillus* TyrDC, respectively, are indicated.

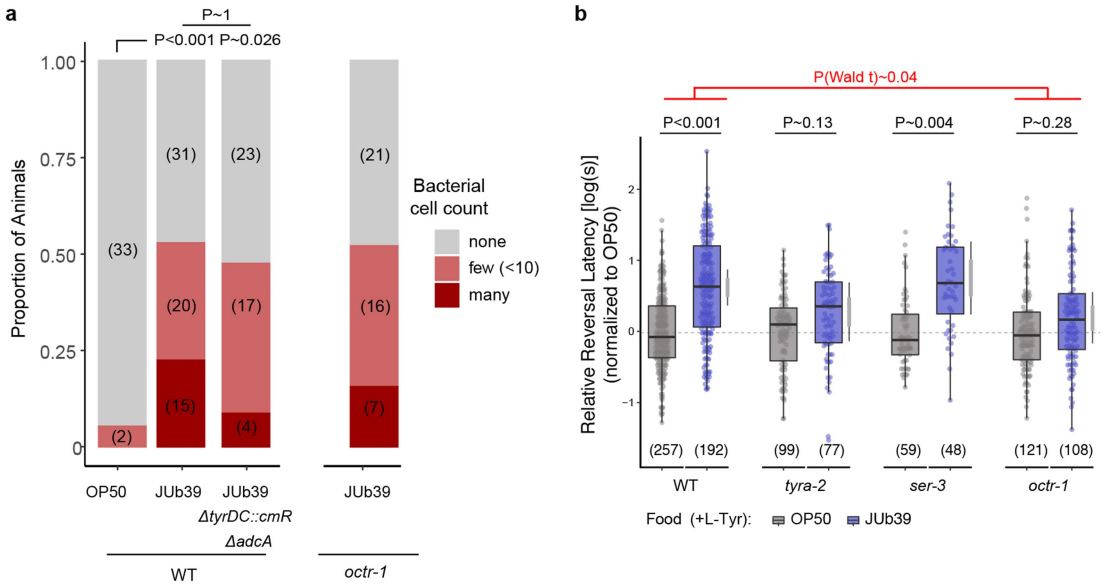


**Extended Data Fig. 9 | Disruption of JUb39 tyramine production or host octopamine receptor signalling affects octanol modulation without altering intestinal bacterial cell numbers. a**, Presence of mCherry-expressing bacteria in the posterior intestines of young adult wild-type or *octr-1*-mutant worms. Bars show proportion of worms with the indicated distribution of bacterial cells present in worms grown on the bacteria indicated. Numbers in parentheses, number of worms. *P* value is derived from an ordinal regression. **b**, Reversal response latency of worms of the indicated genotypes grown on the bacteria indicated in control conditions of NGM + 0.5% L-Tyr to 100% octanol using SOS assays. Dots, response time of single worms. *Y* axis is $\log_{10}$-scaled for these log-normally distributed data, and normalized to the indicated control group for each experimental day. Numbers in parentheses, number of worms tested in assays over at least three independent days. Box plot, median and quartiles; whiskers, data range (excluding outliers). Grey thin and thick vertical bars, Bayesian 95% and 66% credible intervals for the difference of means, respectively. *P* values between indicated conditions are from an LMM with Tukey-type multivariate *t* adjustment. *P* values in red indicate Wald *t*-statistic representing the genotype × food interaction effect relative to wild type.

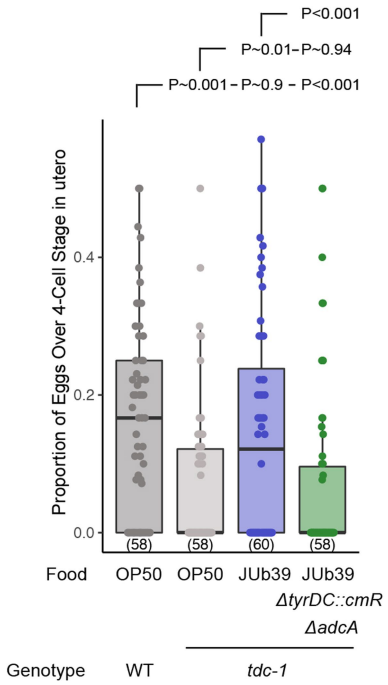


**Extended Data Fig. 10 | *Providencia*-derived tyramine complements the egg-laying defects of *tdc-1*-mutant *C. elegans*.** Quantification of the age of eggs in utero of worms of the indicated genotypes, grown on the indicated bacterial strains. Dots, proportion of eggs at or older than the four-cell stage in individual worms. Numbers in parentheses, total number of worms scored in three independent experiments. Box plot, median and quartiles; whiskers, data range (excluding outliers). *P* values between the indicated conditions are from a binomial generalized linear mixed effects regression using a logit link function, with a post hoc Tukey correction for multiple comparisons.

nature research

Corresponding author(s): Piali Sengupta
Michael O'Donnell

Last updated by author(s): Mar 9, 2020

# Reporting Summary

Nature Research wishes to improve the reproducibility of the work that we publish. This form provides structure for consistency and transparency in reporting. For further information on Nature Research policies, see Authors & Referees and the Editorial Policy Checklist.

## Statistics

For all statistical analyses, confirm that the following items are present in the figure legend, table legend, main text, or Methods section.

| n/a | Confirmed |
|---|---|
| ☐ | ☒ The exact sample size (*n*) for each experimental group/condition, given as a discrete number and unit of measurement |
| ☐ | ☒ A statement on whether measurements were taken from distinct samples or whether the same sample was measured repeatedly |
| ☐ | ☒ The statistical test(s) used AND whether they are one- or two-sided<br>*Only common tests should be described solely by name; describe more complex techniques in the Methods section.* |
| ☐ | ☒ A description of all covariates tested |
| ☐ | ☒ A description of any assumptions or corrections, such as tests of normality and adjustment for multiple comparisons |
| ☐ | ☒ A full description of the statistical parameters including central tendency (e.g. means) or other basic estimates (e.g. regression coefficient) AND variation (e.g. standard deviation) or associated estimates of uncertainty (e.g. confidence intervals) |
| ☐ | ☒ For null hypothesis testing, the test statistic (e.g. *F*, *t*, *r*) with confidence intervals, effect sizes, degrees of freedom and *P* value noted<br>*Give P values as exact values whenever suitable.* |
| ☐ | ☒ For Bayesian analysis, information on the choice of priors and Markov chain Monte Carlo settings |
| ☐ | ☒ For hierarchical and complex designs, identification of the appropriate level for tests and full reporting of outcomes |
| ☒ | ☐ Estimates of effect sizes (e.g. Cohen's *d*, Pearson's *r*), indicating how they were calculated |

*Our web collection on statistics for biologists contains articles on many of the points above.*

## Software and code

Policy information about availability of computer code

| | |
|---|---|
| Data collection | Vanquish LC system controlled by Chromeoleon Software v7.2.9 (ThermoFisher Scientific) and coupled to an Orbitrap Q-Exactive High Field mass spectrometer controlled by Xcalibur software v4.1.31.9 (ThermoFisher Scientific). |
| Data analysis | R version 3.6.0, Rstudio 1.3.158, Canu v1.8, Circlator v1.5.5, MUSCLE v3.8.31, MAFFT v7.407, Kalign v2.04, trimAL v1.4rev15, PhyML v3.3.20180621, tblastn 2.7.1+, ProtTest, Chimera v1.13.1, Metaboseek doi: 10.5281/zenodo.3360087 |

For manuscripts utilizing custom algorithms or software that are central to the research but not yet described in published literature, software must be made available to editors/reviewers. We strongly encourage code deposition in a community repository (e.g. GitHub). See the Nature Research guidelines for submitting code & software for further information.

## Data

Policy information about availability of data

All manuscripts must include a data availability statement. This statement should provide the following information, where applicable:

- Accession codes, unique identifiers, or web links for publicly available datasets
- A list of figures that have associated raw data
- A description of any restrictions on data availability

All statistical analysis code and data necessary to reproduce these analyses are available as uploaded Source Data and/or at https://github.com/SenguptaLab/ProvidenciaChemo.git. Raw data from HPLC-MS experiments are available upon request due to large file sizes.

# Field-specific reporting

Please select the one below that is the best fit for your research. If you are not sure, read the appropriate sections before making your selection.

☒ Life sciences ☐ Behavioural & social sciences ☐ Ecological, evolutionary & environmental sciences

For a reference copy of the document with all sections, see nature.com/documents/nr-reporting-summary-flat.pdf

# Life sciences study design

All studies must disclose on these points even when the disclosure is negative.

| | |
|---|---|
| Sample size | Sample sizes for behavioral experiments and fluorescence imaging were chosen based on conventional estimates of power for these assays. |
| Data exclusions | No data were excluded. |
| Replication | Data from principle findings in the manuscript were reproduced repeatedly in the manuscript. All behavioral experiments were generally repeated over a minimum of 3 experimental days. |
| Randomization | Randomization is not relevant to this study. Covariates, pseudoreplication and non-independence of observations were accounted for statistically using mixed-effects regression and mixed-effects Bayesian analysis. |
| Blinding | All chemotaxis experiments were scored blind to the condition and genotype of the animals. Blinding was not practical for other experiments in the manuscript. |

# Reporting for specific materials, systems and methods

We require information from authors about some types of materials, experimental systems and methods used in many studies. Here, indicate whether each material, system or method listed is relevant to your study. If you are not sure if a list item applies to your research, read the appropriate section before selecting a response.

## Materials & experimental systems

| n/a | Involved in the study |
|---|---|
| ☒ | ☐ Antibodies |
| ☒ | ☐ Eukaryotic cell lines |
| ☒ | ☐ Palaeontology |
| ☐ | ☒ Animals and other organisms |
| ☒ | ☐ Human research participants |
| ☒ | ☐ Clinical data |

## Methods

| n/a | Involved in the study |
|---|---|
| ☒ | ☐ ChIP-seq |
| ☒ | ☐ Flow cytometry |
| ☒ | ☐ MRI-based neuroimaging |

## Animals and other organisms

Policy information about studies involving animals; ARRIVE guidelines recommended for reporting animal research

| | |
|---|---|
| Laboratory animals | C. elegans adult hermaphrodites used for all behavioral experiments. |
| Wild animals | Wild nematodes were captured from compost and were lysed to isolate bacteria (Fig. 1b and Extended Data Fig. 1c). These animals were not subsequently used in the study. |
| Field-collected samples | Samples collected from compost were kept at room temperature prior to isolation. |
| Ethics oversight | No ethical oversight organization was necessary for use of C. elegans. |

Note that full information on the approval of the study protocol must also be provided in the manuscript.